Abstract

Contents

Chapter 2

Numerical Techniques

We will discuss the fundamentals of numerical methods relevant to solving the Navier-Stokes equations. We begin the discussion of the weighted of residuals (§2.1) and the spatial discretisation using spectral/*hp* element methods in one dimension (§2.3). This is followed by techniques for solving the Navier-Stokes equations (§2.4), introducing the velocity-correction scheme, enforcing a constant flow rate and the quasi-3D approach for semi-homogeneous domains. This chapter concludes with numerical techniques for the stability analysis of the Navier-Stokes equations (§2.5), including eigenvalue computation and edge tracking.

2.1 Method of weighted residuals

Spatial discretisation errors, or residuals, arises as one seeks an approximate solution to some partial differential equation (PDE). The method of weighted residual provides a generic mathematical framework in which constraints on the residual could be applied flexibly, defining the spatial discretisation scheme and its convergence properties. In summary, we approximate the solution of PDE by considering a finite expansion of a suitable basis, to which its coefficients are sought after by minimising the inner product between the PDE and a test (or weight) function. To demonstrate this, we consider a linear partial differential equation as,

$$\mathbf{L}[u(x)] = 0, \quad x \in \Omega, \tag{2.1}$$

where $\mathbf{L}$ refers to a linear spatial differential operator subjected to some boundary conditions within the domain, Ω, while $u(x)$ refers to the exact solution of $\mathbf{L}$. Examples of PDEs with linear spatial differential operators include the Laplace equation, $\nabla^2 u = 0$, Poisson equation, $\nabla^2 u = f$, and the Helmholtz equation, $\nabla^2 u + \lambda u = f$. We suppose that the exact solution $u(x)$ can be approximated (discretised) by N finite number of basis (or expansion) functions, $\Phi(x)$.

$$u(x) \approx u^{\delta}(x) = \sum_{i=0}^{N-1} \hat{u}_i \Phi_i(x), \tag{2.2}$$

where $u^\delta(x)$ refers to the approximate solution of $u(x)$, consisting of a linear combination of the product between the i^{th} basis coefficient, $\hat{u}_i$, and the i^{th} global basis expansion, $\Phi_i(x)$, defined within Ω. Since $u^\delta(x)$ is an approximate solution of equation (2.5), we expect a residual (or 'error') between the exact solution, $u(x)$, and $u^\delta(x)$,

$$\mathbf{L}[u^\delta(x)] = R[u^\delta(x)], \tag{2.3}$$

where $R[u^\delta(x)]$ refers to the residual which depends on the approximate solution $u^\delta(x)$ and varying within Ω. In other words, equation (2.5) might not be satisfied everywhere in Ω. We need to place restrictions on the residual, such that it the residual approaches zero, $R \to 0$, and the approximate solution approaches the exact solution, $u^\delta(x) \to u(x)$. The method of residuals places a restriction on the residual by applying an inner product between the governing equation, and N test (or weight) functions, $v_j(x)$, and setting it to zero,

$$(v_j(x), R[u^\delta(x)]) = 0, \quad j = 0, ..., N-1. \tag{2.4}$$

Definition 2.1.1 (Inner product)**.** The inner product between two functions $f(x)$ and $g(x)$ is,

$$(f, g) = \int_\Omega f(x)g(x)dx.$$

By setting equation (2.4) to zero, it becomes a system of N ordinary differential equations, where the N basis coefficients, $\hat{u}_i$. The choice of test function defines the projection methods, and examples of projection methods are shown in table 2.1. We emphasise that the method of weighted residuals merely describes the projection method, but does not specify the type of basis expansions, as we will discuss later in §2.3. The choice of projection method coupled with suitable basis expansions will have different solution convergence properties. A particular interest is on how quickly the residual vanishes as the number of basis expansions increases. For instance, by considering the Galerkin method coupled with Fourier expansions, one can expect exponential convergence, desirable for an efficient representation of turbulent dynamics.

Weight functions	Projection method
$v_j(x) = \delta(x - x_j)$	Collocation
$v_j(x) = \begin{cases} 1 & \text{if } x \in \Omega_j \\ 0 & \text{if } x \notin \Omega_j \end{cases}$	Finite-Volume
$v_j(x) = \phi_j$	Galerkin
$v_j(x) = \frac{\partial R}{\partial \hat{u}_j}$	Least-squares

Table 2.1: Examples of weight functions and projection methods

2.2 Galerkin Projection

The Galerkin projection remains a standard projection method in the context of the finite element method, where the test functions, $v(x)$, are chosen to be lie in the same functional space as the global basis functions, $\Phi(x)$. To demostrate the Galerkin projection method, we consider that the differential operator earlier in equation (2.1) as a 1D Helmholtz equation,

$$\mathbf{L}[u(x)] \equiv \frac{\partial^2 u(x)}{\partial x^2} - \lambda u(x) - f(x) = 0, \quad x \in \Omega := [0, l] \tag{2.5a}$$

$$u(0) = g_D, \quad \left.\frac{\partial u}{\partial x}\right|_{x=l} = g_N. \tag{2.5b}$$

where λ is a real positive constant, $f(x)$ is a forcing function, and Ω refers to the spatial domain bounded between 0 and l. To ensure that problem is well posed, Dirichlet and Neumann boundary conditions, g_D and g_N, are imposed at $x = 0$ and $x = l$ respectively. Equation 2.5 is commonly referred to as the strong or classical form.

The subsequent step in Galerkin projection methods is take the inner product of the equation (2.5) with a test function, $v(x)$, that satisfies the homogeneous Dirichlet boundary conditions by definition, i.e. $v(0) = 0$, and setting the inner product to zero,

$$(v(x),\, \mathbf{L}[u(x)]) = \int_0^l w \left[\frac{\partial^2 u(x)}{\partial x^2} - \lambda u(x) + f(x)\right] \mathrm{d}x = 0. \tag{2.6}$$

This step is equivalent to applying the method of weighted residuals (§2.1), where $u(x)$ could refer to the approximate solution, $u^\delta(x)$. Next, we perform integration by parts,

$$\underbrace{\int_0^l \frac{\partial v}{\partial x}\frac{\partial u}{\partial x}\,\mathrm{d}x + \int_0^l \lambda v u\,\mathrm{d}x}_{a(v,u)} = \underbrace{\int_0^l v f\,\mathrm{d}x + \left[v\frac{\partial u}{\partial x}\right]_0^l}_{f(v)}. \tag{2.7}$$

This equation is typically referred to as the weak [1] form of equation (2.5). In compact notation, we define the bilinear and linear forms as,

$$a(v, u) = f(v), \tag{2.8a}$$

where $a(v, u)$ and $f(v)$ are typically refered to as the strain energy and forcing function in structural mechanics, required to remain finite. To ensure this, we restrict the choice of solutions $u(x)$ to lie in the solution space, $\mathcal{U}$, defined as

$$\mathcal{U} := \{u \,|\, u \in H^1(\Omega), u(0) = g_D\}, \tag{2.9}$$

[1] The notions of the *weak* and *strong* are refers to the smoothness (regularity) required of admissible solutions. In the weak formulation, the highest derivative involved is up to first-order, so the solution space is H^1. This space is generally larger than that of the strong formulation, which required $u \in \mathcal{H}^2(\Omega)$. Since $H^2(\Omega) \subset H^1(\Omega)$ the weak formualation imposesd a 'less stringent' constraint of the solution space of admissible functions.

where $u \in H^1$ refers to functions of u belonging to Sobolev space of order 1, and satistfying the Dirichlet condition, $u(0) = g_D$, at $x = 0$.

Definition 2.2.1 (Sobolev space)**.** We define Sobolev space of order $n \geq 1$ on Ω,

$$H^n(\Omega) = \{u \,|\, u \in L_2(\Omega), D^\alpha u \in L_2(\Omega), \forall \alpha : \alpha \leq n\},$$

where $D^\alpha u$ refers to derivatives up to order α and $L_2(\Omega)$ refers to functions that are square integrable.

Definition 2.2.2 (L_2 space)**.** The space $L_2(\Omega)$ refers to functions that are square integrable,

$$(u, u)_{L_2} = \int_\Omega |u(x)|^2 \, \mathrm{d}\Omega < \infty. \tag{2.10}$$

We consider admissible functions up to the first derivatives, the highest order derivative in the weak formulation of equation (2.6). Similarly, the space of test functions, $\mathcal{V}$, is defined as,

$$\mathcal{V} := \{v \,|\, v \in H^1, v(0) = 0\}, \tag{2.11}$$

where $v \in H^1$ are refer to test functions belonging to the Sobolev the space of order 1, and is defined to be zero, $v(0) = 0$ on Dirichlet boundary condition, $x = 0$. The generalised weak form is therefore finding $u(x) \in \mathcal{U}$, such that

$$a(v, u) = f(v), \quad \forall v \in \mathcal{V}. \tag{2.12}$$

At this point, equation (2.12) is infinite dimension as the function spaces, $\mathcal{U}$ and $\mathcal{V}$, contain infinitely many functions. To obtain an approximate solution, $u^\delta(x)$, we restrict ourselves to finite dimensional subspaces, $\mathcal{U}^\delta \subset \mathcal{U}$, and $\mathcal{V}^\delta \subset \mathcal{V}$. The problem is then to find $u^\delta \in \mathcal{U}^\delta$, such that

$$a(v^\delta, u^\delta) = f(v^\delta), \quad v^\delta \in \mathcal{V}^\delta. \tag{2.13}$$

Here, the subspaces $u^\delta \in \mathcal{U}^\delta$ and $v^\delta \in \mathcal{V}^\delta$ are not the same, compare equations (2.9) and (2.11), necessary for the standard Galerkin projection procedure where they should lie in the same subspace. To ensure that they belong to the same space, we lift the solution u^δ into two parts,

$$u^\delta = u^\mathcal{H} + u^\mathcal{D}. \tag{2.14}$$

where $u^\mathcal{H} \in \mathcal{V}^\delta$ satisfies the homogeneous Dirichlet condition (e.g. is zero on Dirichlet boundaries), belonging to the same subsapce as $v^\delta \in \mathcal{V}^\delta$, while $u^\mathcal{D} \in \mathcal{U}^\delta$ satisfies the Dirichlet boundary conditions $u^\mathcal{D}(0) = g_D$. Hence, the standard Galerkin projection method is to search for the homogeneous solution, $u^\mathcal{H} \in \mathcal{V}^\delta$, such that,

$$a(v^\delta, u^\mathcal{H}) = f(v^\delta) - a(v^\delta, u^\mathcal{D}). \tag{2.15}$$

This concludes the classical Galerkin formulation. Under certain assumptions of a, a solution is guaranteed under the Lax-Milgram theorem [Lax and Milgram, 1955].

2.3 Spectral/*hp* element methods

We have described the procedure for approximating a solution of a PDE using the classical Galerkin projection technique. However, the spatial discretisation scheme, related to the choice of basis (and test) functions, remains undiscussed. In this section, we discuss the spectral/*hp* element method [Patera, 1984], where the solution is partitioned into a set of non-overlapping finite elements of size h, consisting of a linear combinbation of continuous orthogonal polynomial functions up to order P. It leverages the geometric flexibility of classical finite-element methods, allowing for the representation of complex engineering geometries, and the exponential (spectral) convergence properties of classical spectral methods, where the solution error decreases exponentially. Suppose we consider $P+1$ linearly independent polynomials spanning the polynomial space of $\mathcal{P}_P$, the error of a smooth solution with element size of h and polynomial order P has the property of [Karniadakis and Sherwin, 2005],

$$||u(x) - u^{\delta}(x)|| \leq Ch^P ||u(x)|| \approx O(h^P). \tag{2.16}$$

where C is some constant. Equation 2.16 implies that the error decreases linearly with h, and exponentially with P. This section is organised into domain partition, standard elements, assembly process, modal and nodal expansion functions, numerical integration and differentiation, concluding with an example in 1D.

2.3.1 Domain partition

The first step concerns the partitioning the domain into a set of (finite) elemental regions. We consider an example in one dimension within Ω, and partition it into a set of N_{el} elements, where Ω^e, refers to the elemental partitions with $1 \geq e \geq N_{el}$, such that they meet at their boundaries and do not overlap,

$$\Omega = \bigcup_{e=1}^{N_{el}} \Omega^e, \quad \text{where} \bigcap_{e=1}^{N_{el}} \Omega^e = \emptyset \tag{2.17}$$

where the e^{th} element is defined as,

$$\Omega^e = \{x \,|\, x_{e-1} \geq x \geq x_e\}. \tag{2.18}$$

Each element can be represented by a linear combination of orthogonal basis expansions. The basis expansions can be either modal or nodal expansions, as we shall see later.

2.3.2 Standard Elements

In general, we expect to work with non-uniform elements that may have arbitrarily shapes, making the definition of basis expansions potentially unwieldy. To simplify the formulation, it is convenient to define a *standard* element,

$$\Omega_{st} = \{\xi \,|\, -1 \geq \xi \geq 1\}, \tag{2.19}$$

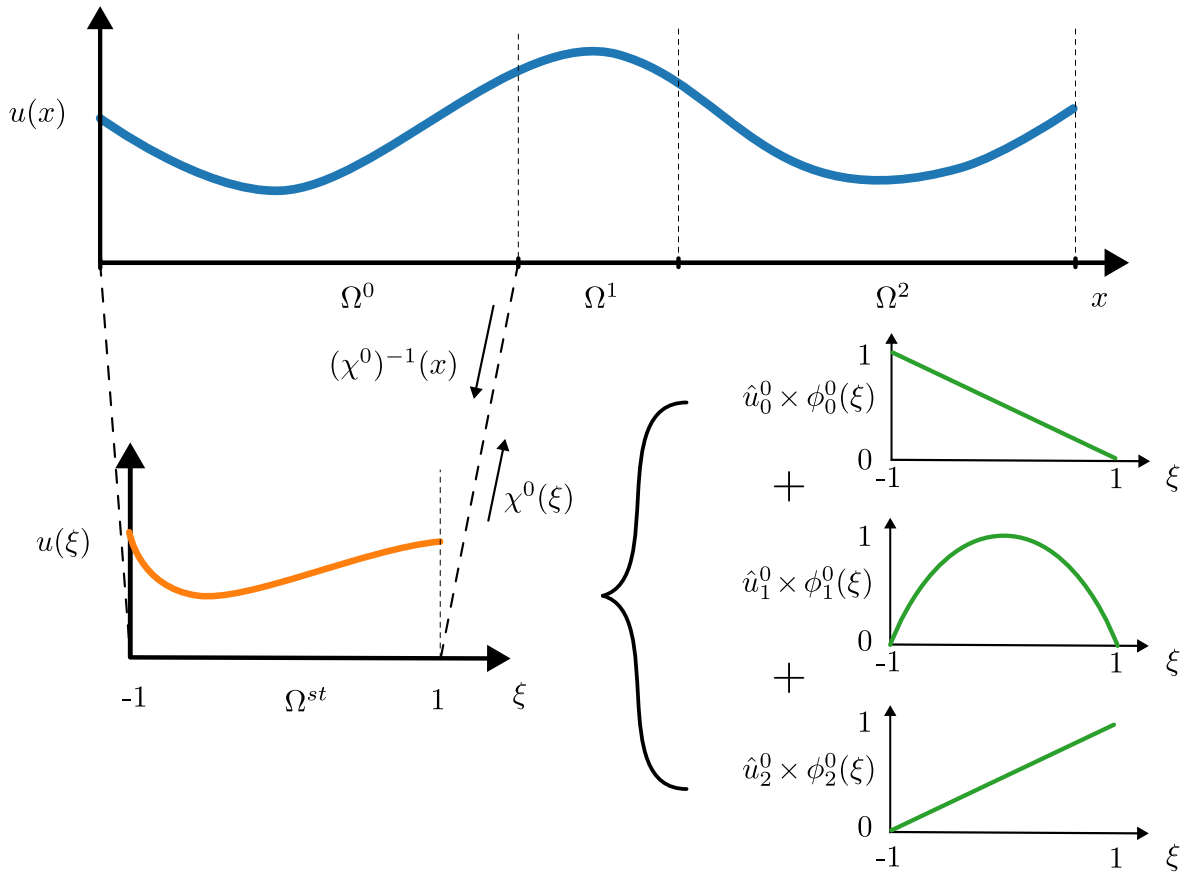

Figure 2.1: A spectral/*hp* element representation of $u(x)$, consisting of three non-overlapping finite elements, each containing a linear combination of local expansion bases of up to $P = 2$.

where Ω_{st} refers to the standard element defined in local coordinates, $\xi \in [-1, 1]$. Within this standard element, the formulation of basis expansions, as well as differential and integration operations, can be carried out in the local coordinate system ξ, before mapping the solution back to the global domain, x. We can map the standard element into any arbitrary global coordinates based on a linear mapping $\chi^e : \Omega_{st} \to \Omega$,

$$x = \chi^e(\xi) = \frac{1-\xi}{2} x_e + \frac{1+\xi}{2} x_{e+1}, \quad \xi \in \Omega_{st} \tag{2.20}$$

which has an analytical inverse, $(\chi^e)^{-1}(x)$,

$$\xi = (\chi^e)^{-1}(x) = 2\frac{x - x_{e-1}}{x_e - x_{e-1}} - 1, \quad x \in \Omega^e. \tag{2.21}$$

For illustration purposes, we consider that the standard element can be represented by three local basis expansions of polynomial order of up to $P = 2$,

$$\phi_0^e(\xi) = \frac{1-\xi}{2}, \quad \phi_1^e(\xi) = (1+\xi)(1-\xi), \quad \phi_2^e(\xi) = \frac{1+\xi}{2}, \tag{2.22}$$

where ϕ_0^e, ϕ_2^e and ϕ_1^e refers to the linear and quadratic local basis expansions of the e^{th} element. These local basis expansions is illustrated in figure 2.1. We note that the formulations of local basis

expansion here is merely an example. In practice, the local basis expansions are usually chosen to have orthogonality properties under a certain inner product. The approximate solution is now represented as,

$$u^{\delta}(x) = \sum_{e=0}^{N_{el}-1} \sum_{i=0}^{P} \hat{u}_i^e \phi_i^e(\chi^e(\xi)). \tag{2.23}$$

where $\hat{u}_i^e$ refers to the local expansion basis coefficients. The approximate solution, $u^{\delta}(x)$, now lie within the solution space $\mathcal{U}^{\delta}$ defined as,

$$\mathcal{U}^{\delta} := \left\{ u^{\delta} \,\middle|\, u^{\delta} \in H^1,\ u^{\delta}(\chi^e(\xi)) \in \phi_i^e(\xi), \forall i : 0 \leq i \leq P, \forall e : 0 \leq e \leq N_{el} \right\} \tag{2.24}$$

2.3.3 Global assembly

In this section, we introduce the concept of global assembly (or direct stiffness summation) which relates the global basis expansions (equation (2.2)), $\Phi_i(x)$, to the local basis expansions (equation (2.23)), $\phi_i^e(x)$, where the solution can be approximated using either formulation,

$$u^{\delta}(x) = \sum_{i=0}^{N-1} \hat{u}_i \Phi_i(x) = \sum_{e=0}^{N_{el}-1} \sum_{i=0}^{P} \hat{u}_i^e \phi_i^e(\chi^e(\xi)). \tag{2.25}$$

In general, we can represent the global and local basis coefficients each as a column vector,

$$\hat{\mathbf{u}}_g = \begin{pmatrix} \hat{u}_0 \\ \vdots \\ \hat{u}_N \end{pmatrix}, \quad \hat{\mathbf{u}}_l = \begin{pmatrix} \hat{\mathbf{u}}^0 \\ \vdots \\ \hat{\mathbf{u}}^{N_{el}-1} \end{pmatrix}, \tag{2.26}$$

where $\hat{\mathbf{u}}^e = (\hat{u}_0^e, ..., \hat{u}_P^e)^T$, $\hat{\mathbf{u}}_g \in \mathbb{R}^N$, $\hat{\mathbf{u}}_l \in \mathbb{R}^{N_{loc}}$ and $N_{loc} = N_{el}(P+1)$. As there can be more global degrees of freedom than local degrees of freedom, $N > N_{loc}$, we need to impose some conditions on the local expansion coefficients. One of the common approach is to enforce C^0 continuity across elemental boundaries, referred to as the continous Galerkin projection. Following the definition of local basis expansions in equation (2.22), this condition can be supplemented using,

$$\hat{u}_P^{e-1} = \hat{u}_0^e. \tag{2.27}$$

The graphical representation of this condition enforcing C^0 continuity between the element boundaries for three finite elements with $P = 2$ local basis expansions, and the relationship between global and local basis coefficients are shown in figure 2.2. We can relate the global and local basis coefficients with an assembly matrix, $\mathbf{A} \in \mathbb{R}^{N_{loc} \times N}$,

$$\hat{\mathbf{u}}_l = \mathbf{A}\hat{\mathbf{u}}_g. \tag{2.28}$$

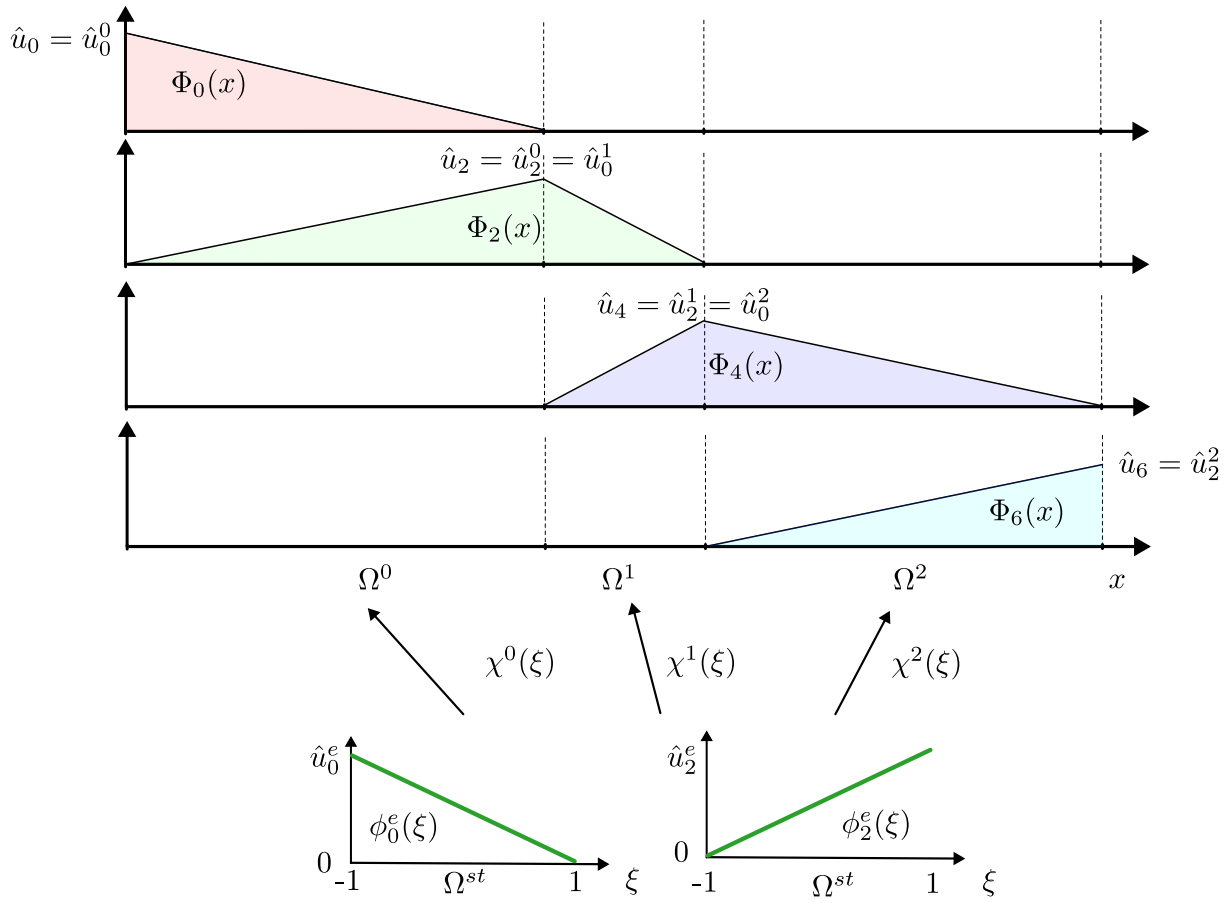

Figure 2.2: A graphical representation of C^0 across elemental boundaries and the relationship between local basis coefficients, u_0^e, u_P^e, and global basis expansions, u_i.

In the case for $P = 2$ and three finite elements as in the case of figures 2.1and 2.2, the assembly matrix and the vectors of global and local basis coefficients are given as,

$$\hat{\mathbf{u}}_l = \begin{pmatrix} \hat{u}_0^0 \\ \hat{u}_1^0 \\ \hat{u}_2^0 \\ \hat{u}_0^1 \\ \hat{u}_1^1 \\ \hat{u}_2^1 \\ \hat{u}_0^2 \\ \hat{u}_1^2 \\ \hat{u}_2^2 \end{pmatrix}, \quad \mathbf{A} = \begin{pmatrix} 1\,0\,0\,0\,0\,0\,0 \\ 0\,1\,0\,0\,0\,0\,0 \\ 0\,0\,1\,0\,0\,0\,0 \\ 0\,0\,1\,0\,0\,0\,0 \\ 0\,0\,0\,1\,0\,0\,0 \\ 0\,0\,0\,0\,1\,0\,0 \\ 0\,0\,0\,0\,1\,0\,0 \\ 0\,0\,0\,0\,0\,1\,0 \\ 0\,0\,0\,0\,0\,0\,1 \end{pmatrix}, \quad \hat{\mathbf{u}}_g \begin{pmatrix} \hat{u}_0 \\ \hat{u}_1 \\ \hat{u}_3 \\ \hat{u}_4 \\ \hat{u}_5 \\ \hat{u}_6 \end{pmatrix}, \tag{2.29}$$

The assembly matrix $\mathbf{A}$ 'scatters' the global degrees of freedom to local degrees of freedom, while the transpose of it, $\mathbf{A}^T$, performs the reverse, referred to as global assembly. For example, we wish to perform integration in the domain Ω,

$$\mathbf{I}_g[j] = (\Phi_j(x), u^\delta(x)), \tag{2.30}$$

where $\mathbf{I}_g \in \mathbb{R}^N$ refers to a vector containing the integral between $\Phi_i(x)$ and $u^\delta(x)$. This is related to first performing integration using local expansion basis within standard elements, and then assembling using $\mathbf{A}^T$,

$$\mathbf{I}_g = \mathbf{A}^T \mathbf{I}_l, \tag{2.31a}$$

where,

$$\mathbf{I}_g = \begin{bmatrix} \mathbf{I}_0 \\ \vdots \\ \mathbf{I}_{N_g-1} \end{bmatrix}, \quad \mathbf{I}_l = \begin{bmatrix} \mathbf{I}^0 \\ \vdots \\ \mathbf{I}^{N_{el}-1} \end{bmatrix}, \quad \text{with} \quad \mathbf{I}^e = \begin{bmatrix} \int_{-1}^{1} \phi_0^e(\xi) u(\chi^e) \frac{\mathrm{d}\chi^e}{\mathrm{d}\xi} \, \mathrm{d}\xi \\ \vdots \\ \int_{-1}^{1} \phi_{P-1}^e(\xi) u(\chi^e) \frac{\mathrm{d}\chi^e}{\mathrm{d}\xi} \, \mathrm{d}\xi \end{bmatrix}, \tag{2.31b}$$

and $\mathbf{I}_l \in \mathbb{R}^{N_{loc}}$ refer to the vector of integration operations performed within a standard element. In the spectral/*hp* element approach, we perform integration and differentiation using local basis expansions within a standard element. After doing so, we assemble the local operations from the standard element to the global domain by using $\mathbf{A}^T$, as we shall show later using a 1D example. We note that the structure of assembly matrix is generally sparse, where the entries either contain 0, 1 or -1 in multidimensional formulation. Therefore, the assembly matrix is not constructed in practice, and a mapping array is used instead.

2.3.4 Local basis expansions

The choice of local basis expansions, $\phi_i^e(\xi)$, pertains the representation of the solution, and the convergence properties of the numerical solver, in particular, the condition number of the mass and laplacian matrices. In general, the the local basis expansions can be classified into two groups, either *modal* or *nodal* expansions.

Modal expansions

Modal expansions, or hierarchical expansions, describes a set of expansion basis where an expansion set of order $P-1$, $\mathcal{X}_{P-1}^\delta$, is contained within a set of order P, $\mathcal{X}_P^\delta$, e.g. $\mathcal{X}_{P-1}^\delta \subset \mathcal{X}_P^\delta$. The Jacobi polynomials, $P_p^{\alpha,\beta}(x)$, representing a family of solutions with arbitrary values of (α, β) to the Sturm-Liouville problem within, $x \in [-1, 1]$, are modal expansions. Notably, the Legendre polynomials are a special case of Jacobi polynomials, $L_n(\xi) = P_n^{0,0}(\xi)$ with $\alpha = \beta = 1$. Within the Nektar++ framework, it is common to use the *modified* basis based on Jacobi polynomials, $P_p^{\alpha,\beta}(\xi)$ which are modified with linear elements as

$$\phi_p(\xi) = \psi_p(\xi) = \begin{cases} \frac{1-\xi}{2} & \text{for } p = P \\ \frac{1-\xi}{2}\frac{1+\xi}{2} P_{P-1}^{1,1}(\xi) & \text{for } P \geq 2 \\ \frac{1+\xi}{2} & \text{for } p = P, \end{cases} \tag{2.32}$$

where P denotes the highest polynomial order. Figure 2.3 shows the modified Jacobi polynomials for $p \in [0, 5]$ described by equation 2.32. The boundary modes are ψ_0 and ψ_5 while the rest are boundary modes.

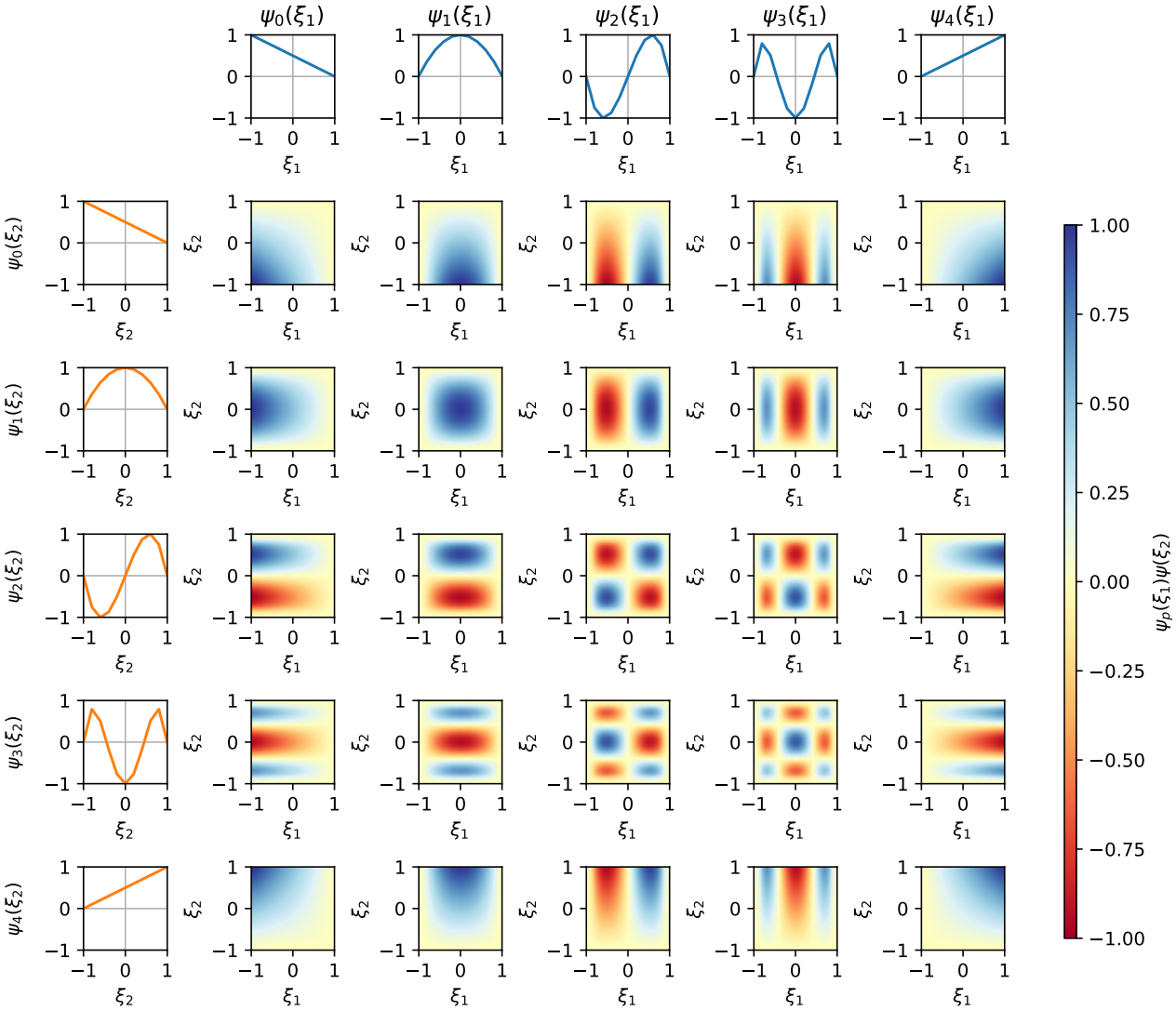

Figure 2.3: Two-dimensional and one-dimension modified basis, $\psi_p(\xi_1)$ and $\psi_q(\xi_2)$, $P = [0, 4]$.

Nodal expansions

Nodal expansions are basis expansions that are non-hierchical, $Lagrange polynomials are an example of nodal exp$ $h_p(\xi) = \frac{\prod_{q=0,q\neq p}^{P}(\xi-\xi_q)}{\prod_{q=0,q\neq p}^{P}(\xi_p-\xi_q)}$(2.33)The Lagrange polynomials are particular attractive as it has a unit value at ξ_q and zero everywhere else, $h_p(\xi_q) = \delta_{pq}$, which implies that

$$u^{\delta}(\xi_q) = \sum_{p=0}^{P} \hat{u}_p h_p(\xi_q) = \sum_{p=0}^{P} \hat{u}_p \delta_{pq} = \hat{u}_q, \tag{2.34}$$

where the Lagrange coefficient $\hat{u}_q$ is the same as the value evaluted at the node ξ_q, hence referred to nodal expansions. Typically, the zeros are located using the zeros of the Gauss-Lobatto polynomials

where the zeros are defined using

$$\phi_p(\xi) \to h_p(\xi) = \begin{cases} 1, & \xi = \xi_p, \\ \frac{(\xi^2-1)[P^{\alpha,\beta}_{Q-1}(\xi)]'}{(Q-1)(Q+\alpha+\beta)P^{\alpha,\beta}_{Q-1}(\xi_j)(\xi-\xi_j)}, & \text{otherwise.} \end{cases} \tag{2.35}$$

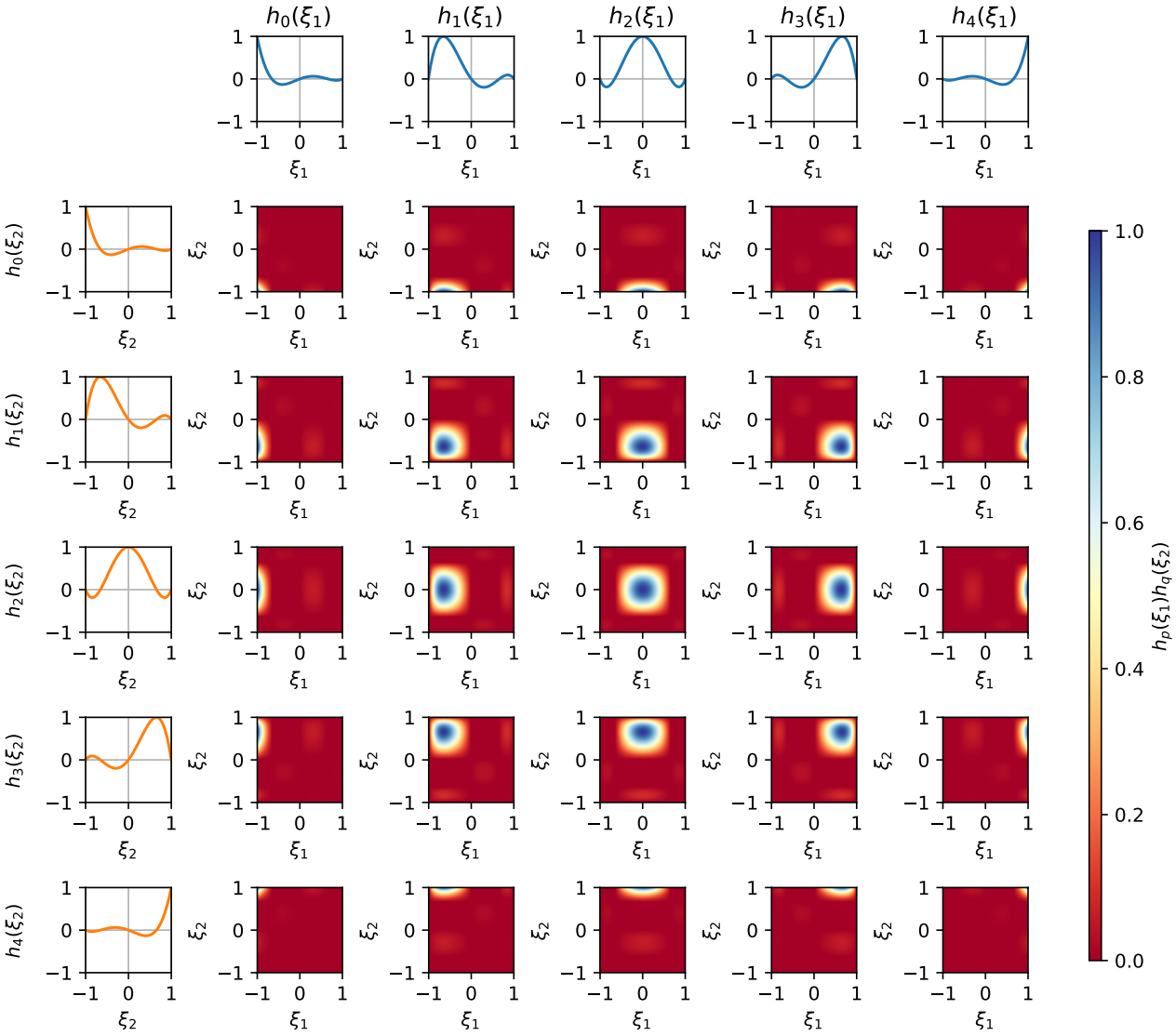

Figure 2.4: Two-dimensional and one-dimension Lagrange basis, $h_p(\xi_1)$ and $h_q(\xi_2)$, $P = [0, 4]$.

Figure 2.4 presents nodal expansions based on two-dimensional and one-dimensional Lagrange polynomials, $h_p(\xi_1), h_q(\xi_2)$ respectively.

2.3.5 Numerical integration

In the Galerkin formulation, we perform integration routinely. Suppose we want to approximate the integral of a smooth function in a standard element numerically,

$$\int_{-1}^{1} u(\xi)\ \mathrm{d}\xi = \sum_{i=0}^{Q-1} w_i u(\xi_i) + R(u), \tag{2.36}$$

where $Q, w_i, \xi_i, R(u)$ refers to the quadrature points, integration weights and zeros (or abscissae) and the integral of the error. By evaluating the integral, how are we able to minimise the integral error, $R(u)$, with the least number of quadrature points, Q, at some weights and zeros. If $u(\xi)$ is of polynomial order P, we can expect we might need at least $P+1$ equipspaced points to accurately represent the function and evalute its integral, a rather inefficient method. Gaussain quadrature is allow us to approximate an integral of a function of order P with far lesser thatn $P+1$ points, as we shall see later. The three generic types of Gaussian quadrature rules are known as: Gauss, Gauss-Radau and Gauss-Lobatto. The main difference between the three methods are in the treatment of the zeros, where Gauss quadrature uses zeros without the end points $\xi = \pm 1$. Gauss-Radau quadrature either select one of the end points, usually at $\xi = -1$, and Gauss-Lobatto consider the end points. We will only focus on describing the Gauss-Lobatto quadrature rules and the zeros of Jacobi polynomials known as the Gauss-Lobatto-Jacobi quadrature rules given as,

$$\xi_i^{\alpha,\beta} = \begin{cases} -1 & i = 0, \\ \xi_{i-1,Q-2}^{\alpha+1,\beta+1} & i = 1, ..., Q-2, \\ 1, & i = Q-1, \end{cases} \tag{2.37a}$$

$$w_i^{\alpha,\beta} = \begin{cases} (\beta+1)C_{0,Q-2}^{\alpha,\beta}, & i = 0, \\ C_{i,Q-2}^{\alpha,\beta}, & i = 1, ..., Q-2, \\ (\alpha+1)C_{Q-1,Q-2}^{\alpha,\beta}, & i = Q-1, \end{cases} \tag{2.37b}$$

$$C_{i,Q-2}^{\alpha,\beta} = \frac{2^{\alpha+\beta+1}\Gamma(\alpha+Q)\Gamma(\beta+Q)}{(Q-1)(Q-1)!\Gamma(\alpha+\beta+Q+1)[P_{Q-1}^{\alpha,\beta}(\xi_i)]^2} \tag{2.37c}$$

where $w_i^{\alpha,\beta}, \xi_i^{\alpha,\beta}$ are the zeros and weights of the Gauss-Lobatto-Jacobi quadrature rules, and Γ refers to the Gamma function. By using these conventions, we can obtain an exact integral of a continuous function, $u(\xi)$ of polynomial P, with at least $Q \geq (P+3)/2$ quadrature points.

2.3.6 Numerical differentiation

In the same fashion as Gaussian quadrature, we want to numerical differentiate efficiently, a crucial step in the weak formulation of the Helmholtz equations. Suppose that we want to differentiate in x

using local coordinates given as,

$$\frac{\mathrm{d}u^{\delta}(\xi)}{\mathrm{d}x} = \frac{\mathrm{d}u^{\delta}(\xi)}{\mathrm{d}\xi}\frac{\mathrm{d}\xi}{\mathrm{d}x} = \sum_{p=0}^{P} \hat{u}_p \frac{\mathrm{d}\phi_p(\xi)}{\mathrm{d}\xi}\frac{\mathrm{d}\xi}{\mathrm{d}x}, \tag{2.38}$$

where $\mathrm{d}\xi/\mathrm{d}x$ is simply the Jacobian and the main step in differentiation is in evaluting $\mathrm{d}\phi_p(\xi)/\mathrm{d}\xi$. Now suppose that we express the solution of polynomial order P with Lagrange polynomials, the derivative of the solution commutes,

$$\frac{\mathrm{d}u(\xi)}{\mathrm{d}\xi} = \sum_{i=0}^{Q-1} u(\xi_i)\frac{\mathrm{d}}{\mathrm{d}\xi}h_i(\xi), \tag{2.39}$$

where we only require the derivative to be evaluted at the nodal points, resulting in a derivative matrix of,

$$D_{ij} = \frac{\mathrm{d}h_j(\xi)}{\mathrm{d}\xi}\Big|_{\xi=\xi_i}, \tag{2.40}$$

and the derivative of $u(\xi)$ is simply,

$$\frac{\mathrm{d}u(\xi)}{\mathrm{d}\xi}\Big|_{\xi=\xi_i} = \sum_{j=0}^{Q-1} D_{ij}\hat{u}_j. \tag{2.41}$$

A general representation of the differential operator can be presented as

$$D_{ij} = \begin{cases} \frac{p'_Q(\xi_i)}{p'_Q(\xi_j)}\frac{1}{\xi_i-\xi_j}, & i \neq j, \\ \frac{p''_Q(\xi_i)}{2p'_Q(\xi_i)}, & i = j. \end{cases} \tag{2.42}$$

where $p'_Q(\xi), p''_Q(\xi)$ are specific restricted to the quadrature used. For the Gauss-Lobatto-Jacobi quadrature rules used here, these forms could be found in Appendix C.2 in Karniadakis and Sherwin [2005].

2.3.7 Example in 1D

We have outlined the basic formulation of spectral/*hp* element methods in $1D$ and we will describe its solution procedure, where we start from the weak-form of the Helmholtz equation and convert it into a system of linear equations, amenable to be solved with standard numerical linear algebra techniques. We describe the solution steps as follows,

1. Performing numerical differentiation and integration in the standard region

$$\lambda \underbrace{\int_{-1}^{1} v^{\delta} u^{\mathcal{H}}\,\mathrm{d}\xi}_{\mathbf{M}^e\hat{\mathbf{u}}^e} + \underbrace{\int_{-1}^{1} \frac{\partial v^{\delta}}{\partial \xi}\frac{\partial u^{\mathcal{H}}}{\partial \xi}\mathrm{d}\xi}_{\mathbf{L}^e\hat{\mathbf{u}}^e} = \underbrace{\int_{-1}^{1} v^{\delta} f\,\mathrm{d}\xi}_{\hat{\mathbf{f}}^e} \tag{2.43}$$

Elemental mass operator

Here we introduce the elemental mass operator given as $\mathbf{M}^e$,

$$\begin{aligned}\int_{-1}^{1}\sum_{i=0}^{P}\hat{v}_i^e\phi_i^e(\xi)\sum_{i=0}^{P}\hat{u}_i^e\phi_i^e(\xi)\,\mathrm{d}\xi &= \sum_{q=0}^{Q}\left[\sum_{i=0}^{P}\hat{v}_i^e\phi_i^e(\xi_q)\sum_{i=0}^{P}\hat{u}_i^e\phi_i^e(\xi_q)\right]w_q^e \\ &= (\hat{\mathbf{v}}^e)^T(\mathbf{B}^e)^T\mathbf{W}^e\mathbf{B}^e\hat{\mathbf{u}}^e \\ &= \hat{\mathbf{v}}^T\mathbf{M}^e\hat{\mathbf{u}}^e\end{aligned} \tag{2.44}$$

where $\mathbf{M}^e = (\mathbf{B}^e)^T\mathbf{W}\mathbf{B}^e$ refers to the elementral mass matrix, while $\mathbf{B}^e \in \mathbb{R}^{Q-1,P}$ and $\mathbf{W}^e \in \mathbb{R}^{Q-1,Q-1}$ refers to the elemental basis and weight matrices, a diagonal matrix consisting of integration weights, w_q^e, respectively,

$$\mathbf{B}^e = \begin{bmatrix}\phi_0(\xi_0) & \cdots & \phi_P(\xi_0)\\ \vdots & \ddots & \vdots \\ \phi_0(\xi_Q) & \cdots & \phi_P(\xi_Q)\end{bmatrix}, \quad \mathbf{W}^e = \begin{bmatrix}w_0^e & & 0\\ & \ddots & \\ 0 & & w_Q^e\end{bmatrix} \tag{2.45}$$

Elemental laplacian matrices

Now we consider, convert the product of two first-derivatives in to matrix form,

$$\begin{aligned}\int_{-1}^{1}\sum_{i=0}^{P}\hat{v}_i^e\frac{\mathrm{d}\phi_i^e}{\mathrm{d}\xi}\sum_{i=0}^{P}\hat{u}_i^e\frac{\mathrm{d}\phi_i^e}{\mathrm{d}\xi}\,\mathrm{d}\xi &= \sum_{q=0}^{Q}\left[\sum_{i=0}^{P}\hat{v}_i^eD_{qi}^e\phi_i^e(\xi_q)\sum_{i=0}^{P}\hat{u}_i^eD_{qi}^e\phi_i^e(\xi_q)\right]w_q^e \\ &= \hat{\mathbf{v}}^T(\mathbf{B}^e)^T(\mathbf{D}^e)^T\mathbf{W}^e\mathbf{D}^e\mathbf{B}^e\hat{\mathbf{u}}^e \\ &= \hat{\mathbf{v}}^T\mathbf{L}^e\hat{\mathbf{u}}^e\end{aligned} \tag{2.46}$$

where $\mathbf{L}^e = (\mathbf{B}^e)^T(\mathbf{D}^e)^T\mathbf{W}\mathbf{D}^e\mathbf{B}^e$ refers to the elementral Laplacian matrix.

Forcing vector

Lastly, we consider the right-hand side,

$$\begin{aligned}\int_{-1}^{1}\sum_{i=0}^{P}\hat{v}_i^e\phi_i^e(\xi)f^e(\xi)\,\mathrm{d}\xi &= \sum_{q=0}^{P}\sum_{i=0}^{P}\hat{v}_i^e\phi_i^e(\xi_q)f^e(\xi_q)w_q^e, \\ &= \hat{\mathbf{v}}^T(\mathbf{B}^e)^T\mathbf{W}^e\mathbf{f}^e \\ &= \hat{\mathbf{v}}^T\hat{\mathbf{f}}^e,\end{aligned} \tag{2.47}$$

where $\hat{\mathbf{f}}^e$, is referred to the elemental forcing vector. As we consider all of the matrices, the Helmholtz equations in elemental form is simply solving for,

$$[\lambda\mathbf{M}^e + \mathbf{L}^e]\,\hat{\mathbf{u}}^e = \hat{\mathbf{f}}^e. \tag{2.48}$$

If we considered bolting the elements together and the boundary conditions,

$$\lambda \underbrace{\begin{bmatrix} \mathbf{M}^0 + \mathbf{L}^0 & & \mathbf{0} \\ & \ddots & \\ \mathbf{0} & & \mathbf{M}^{N_{el}-1} + \mathbf{L}^{N_{el}-1} \end{bmatrix}}_{\mathbf{M}_l + \mathbf{L}_l} \underbrace{\begin{bmatrix} \hat{\mathbf{u}}^0 \\ \vdots \\ \hat{\mathbf{u}}^{N_{el}-1} \end{bmatrix}}_{\hat{\mathbf{u}}_l} = \underbrace{\begin{bmatrix} \hat{\mathbf{f}}^0 \\ \vdots \\ \hat{\mathbf{f}}^{N_{el}-1} \end{bmatrix}}_{\hat{\mathbf{f}}_l} + \underbrace{\begin{bmatrix} \mathbf{L}^0 g_D \\ \vdots \\ \mathbf{0} \end{bmatrix}}_{\mathbf{g}_D} + \underbrace{\begin{bmatrix} \mathbf{0} \\ \vdots \\ g_N \end{bmatrix}}_{\mathbf{g}_N}, \tag{2.49}$$

where $\mathbf{M}_l, \mathbf{L}_l, \hat{\mathbf{u}}_l, \hat{\mathbf{f}}_l, \mathbf{g}_D, \mathbf{g}_N$ refers to the local mass matrix, local laplacian matrix, and vector of local expansion coefficients , Dirichlet and Neumann boundary conditions. Finally, we can assemble them using the assembly matrix,

$$\mathbf{A}^T(\lambda \mathbf{M}_l + \mathbf{L}_l)\mathbf{A}\hat{\mathbf{u}}_g = \mathbf{A}^T(\hat{\mathbf{f}}^l + \mathbf{g}_D + \mathbf{g}_N), \tag{2.50}$$

We note that we have did not show the formulation for 2D spectral/*hp* elements as it has been abstracted away within nektar++.

2.4 Numerical techniques for solving the Navier-Stokes equations

2.4.1 Velocity Correction Scheme

The spatial discretisation of the Helmholtz operator and its numerical solution procedure has been discussed using the spectral/*hp* element methods. Here, we describe the numerical methods that is used to solve the Navier-Stokes equations given as,

$$\frac{\partial u}{\partial t} + (\mathbf{u} \cdot \nabla)\mathbf{u} = -\nabla p + \nu \nabla^2 \mathbf{u} + \mathbf{f} \tag{2.51a}$$

$$\nabla \cdot \mathbf{u} = 0, \tag{2.51b}$$

with boundary conditions,

$$\mathbf{u} = 0, \quad \text{on } \partial\Omega. \tag{2.51c}$$

Here, the primitive variables are velocity and pressure $(\mathbf{u}, p)$ and we assumed unit density, $\rho = 1$, with the kinematic viscosity appearing as the control parameter. The time evolution of velocity is explicit expressed in equation (2.51a), but does not appear for the pressure, which is coupled to the velocity field, enforcing the incompressibility condition. Several strategies exist for addressing the coupled velocity-pressure fields by

1. Solving the coupled system such as the Uzawa algorithm,
2. Splitting methods,
3. Change of coordinates (vorticity-streamfunction).

We adopt splitting methods, which 'splits' the evolution of the Navier-Stokes equation into independent substeps. These methods, belonging to the broader family of projection methods first introduced by Teman, can be further classified into pressure-correction or velocity-correction schemes. We focus on a high-order velocity-correction scheme. We rewrite the incompressible Navier-Stokes equations in semi-discrete form with using linear and nonlinear operators as,

$$\frac{\partial \mathbf{u}}{\partial t} = \mathbf{N}(\mathbf{u}) - \nabla p + \nu \mathbf{L}(\mathbf{u}), \tag{2.52a}$$

$$\nabla \cdot \mathbf{u} = 0, \tag{2.52b}$$

with boundary conditions,

$$\mathbf{u}|_{\Omega} = 0, \quad \mathbf{u}(t=0) = \mathbf{u}_0. \tag{2.52c}$$

The nonlinear, $\mathbf{N}$, linear, $\mathbf{L}$, operators are obtained from a suitable spatial-discretisation method such as the spectral/*hp* element method. The nonlinear and linear operators are defined as,

$$\mathbf{N}(\mathbf{u}) \equiv -(\mathbf{u}\cdot\nabla)\mathbf{u} = -\frac{1}{2}\left[(\mathbf{u}\cdot\nabla)\mathbf{u} + \nabla\cdot(\mathbf{u}\mathbf{u})\right], \qquad \mathbf{L}(\mathbf{u}) \equiv \nabla^2\mathbf{u}, \tag{2.53}$$

We note that the nonlinear terms are written in the skew-symmetric to minimise aliasing errors [Karniadakis et al., 1991]. To advance the velocity at time step, $\mathbf{u}^n$, to the next time step, $\mathbf{u}^{n+1}$, we integrate equation (2.52) over a time step Δt,

$$\mathbf{u}^{n+1} - \mathbf{u}^n = \underbrace{\int_{t_n}^{t_{n+1}} \mathbf{N}(\mathbf{u})\,\mathrm{d}t}_{\Delta t \sum_{q=0}^{J_e-1} \beta_q \mathbf{N}(\mathbf{u}^{n-q})} - \underbrace{\int_{t_n}^{t_{n+1}} \nabla p\,\mathrm{d}t}_{\Delta t \nabla \bar{p}^{n+1}} + \nu \underbrace{\int_{t_n}^{t_{n+1}} \mathbf{L}(\mathbf{u})\,\mathrm{d}t}_{\Delta t \sum_{q=0}^{J_i-1} \gamma_q \mathbf{L}(\mathbf{u}^{n+1-q})}. \tag{2.54}$$

The velocity correction scheme evaluates the underbraced terms in three successive independently from left to right independently, effectively 'splitting' equation (2.52) from this point onwards. The first step we perform is to extrapolate the advection velocities, by approximating the nonlinear terms using an explicit scheme such as the Adams-Bashforth family of J_e order,

$$\frac{\hat{\mathbf{u}} - \sum_{q=0}^{J_e-1} \alpha_q \mathbf{u}^{n-q}}{\Delta t} = \sum_{q=0}^{J_e-1} \beta_q \mathbf{N}(\mathbf{u}^{n-q}), \tag{2.55}$$

where $\hat{\mathbf{u}}$ is denotes the primary intermediate velocity field desired and α_e, β_e refers to the time integration coefficients for a prescribe J_e-th order, described later. After evaluting $\hat{\mathbf{u}}$, we move onto the second term in equation (2.54), which defines the pressure at time step $n+1$ as,

$$\frac{\hat{\hat{\mathbf{u}}} - \hat{\mathbf{u}}}{\Delta t} = -\nabla p^{n+1}. \tag{2.56}$$

$\hat{\hat{\mathbf{u}}}$ denotes as the secondary intermediate velocity. In this single equation, we seek to obtain two unknown solutions, $\hat{\hat{\mathbf{u}}}$ and p^{n+1}, which is ill-posed, and seek to impose certain restrictions. The

splitting method assumes that the secondary intermediate velocity is divergence free, $\nabla \cdot \hat{\hat{\mathbf{u}}} = 0$, and satisfies the Dirichlet boundary conditions normal to the boundary, $\hat{\hat{\mathbf{u}}} \cdot \mathbf{n} = \mathbf{u}|_{\Omega} \cdot \mathbf{n}$. By considering the assumptions above and the divergence of equation (2.56), we obtain the pressure Poisson equation with the primary intermediate velocity acting as the forcing term,

$$\nabla^2 p^{n+1} = \nabla \cdot \left(\frac{\hat{\mathbf{u}}}{\Delta t} \right) \tag{2.57a}$$

and boundary conditions,

$$\frac{\partial p^{n+1}}{\partial n} = \mathbf{n} \cdot \left(\frac{\hat{\hat{\mathbf{u}}} - \hat{\mathbf{u}}}{\Delta t} \right). \tag{2.57b}$$

While the pressure boundary condition (2.57b) is straightforward to evalute, it is sensitive to large splitting errors [Karniadakis et al., 1991]. To overcome this, we consider a high-order boundary condition of pressure, obtained by taking the normal dot product of equation (2.52),

$$\frac{\partial p^{n+1}}{\partial t} = -\sum_{q=0}^{J_e-1} \beta_q \left[\frac{1}{\Delta t} \mathbf{u}^{n-q} + \nu [\nabla \times (\nabla \times \mathbf{u}^{n-q})] + (\mathbf{u}^{n-q} \cdot \nabla) \mathbf{u}^{n-q} \right] \cdot \mathbf{n}. \tag{2.58}$$

Notably, the linear operator is expressed as $\mathbf{L}(\mathbf{u}) = \nabla(\nabla \cdot \mathbf{u}) - \nabla \times (\nabla \times \mathbf{u})$, favouring numerical stability [Orszag et al., 1986, Karniadakis et al., 1991]. J_e is the order the explicit scheme as in equation (2.55). After solving for the pressure Poisson equation, the secondary intermediate velocity could be subsequently obtained using equation (2.56). After which, we can move onto the final substep in equation (2.54), by solving a Helmholtz equation for $\mathbf{u}^{n+1}$,

$$\frac{\gamma_0 \mathbf{u}^{n+1} - \hat{\hat{\mathbf{u}}}}{\Delta t} = \nu \sum_{q=0}^{J_i-1} \gamma_q \mathbf{L}(\mathbf{u}^{n+1-q}), \tag{2.59}$$

where the linear terms are treated based similar to the family of Adams-Moulton implicit scheme and J_i, γ_q denotes the order of the scheme and time integration coefficients, completing the velocity correction scheme. The time integration coefficients are determined from stiffly stable schemes shown in table 2.2, an improvement from the Adams-family schemes [Karniadakis et al., 1991]. Before we

Coefficients	1^{st} order	2^{nd} order	3^{rd} order
γ_0	1	3/2	11/6
α_0	1	2	3
α_1	0	-1/2	-3/2
α_2	0	0	1/3
β_0	1	2	3
β_1	0	-1	-3
β_2	0	0	1

Table 2.2: Integration coefficient of stiffly stable schemes from Karniadakis et al. [1991].

do so, we have to define the test functional spaces of velocity, $\mathcal{W}$, and pressure $\mathcal{Q}$, defined as,

$$\mathcal{V} := \{ v \,|\, v \in H_0^1(\Omega),\ v|_{\partial\Omega} = 0 \} \tag{2.60a}$$

$$\mathcal{Q} := \{q \,|\, q \in L_0^2(\Omega), \int_\Omega q \,\mathrm{d}x = 0\}. \tag{2.60b}$$

The Dirichlet boundary conditions for the test functional space, $\mathcal{V}$, is consistent with the primitive velocity, $\mathbf{u}$, while the L_0^2 denotes a zero mean instead of homogeneous Dirichlet boundary conditions. The test function space for pressure is a polynomial other lower since derivatives for pressure do not appear in the weak formulation as we shall see below. We neglect the unsteady term, leading to a steady Stokes problem, appearing as the right-hand if we consider time-advacing the solutions,

$$(\nabla \mathbf{v}, \nu \nabla \mathbf{u}) - (\nabla \cdot \mathbf{v}, p) = (\mathbf{v}, \mathbf{f}), \quad \forall \mathbf{v} \in \mathcal{V} \tag{2.61a}$$

$$(q, \nabla \cdot \mathbf{u}) = 0, \quad \forall q \in \mathcal{Q} \tag{2.61b}$$

which is a time-dependent nonlinear partial differential equation, While methods for temporal and spatial discretisation have been discussed, it is not possible to apply these techniques in a straightforward manner to the incompressible Navier-Stokes equations. This is because of the unique role of the pressure field which ensures that the time-dependent velocity field is divergence-free. However, the velocity and the pressure fields form a coupled-system through the continuity and momentum equations which requires the solution of both fields simultaneously. In general, there are 3 ways to deal with velocity-pressure coupling: (1) Coupled methods (*Uzawa* method), (2) Change of variables (streamfunction-vorticity formulation) and (3) Splitting methods which decouples velocity and pressure. The velocity correction scheme (VCS) (**?**), a type of splitting method, decouples the velocity field from the pressure field used in *nektar*++ will be discussed in this section.

2.4.2 Fourier spectral/*hp* modes

Fourier-Chebyshev-Fourier type discretisation have been recognised as preferred method for performing direct numerical simulations (DNS) of transitional or turbulent channel flows [Kim et al., 1987] owing to its efficient representation of the inhomogeneous wall-normal directions and the homogeneous streamwise and spanwise directions, using Chebyshev and Fourier expansions respectively. The Fourier spectral/*hp* element method draws on this approach, where the homogeneous directions is represented by the Fourier expansions while the spectral/*hp* elements. This approach has been commonly referred to as the Quasi-3D or (2.5D) approach, allowing for a flexible description of the inhomogeneous directions, such as riblets [doug chu]. For example, in the turbulent channel flows with riblets, the Fourier expansions are used to represent the periodic streamwise, while the spectral/*hp* elements are used to discretise the wall-normal direction. In the analysis of three-dimensional wakes of cylinders where the Fourier expansions are treated in the spanwise directions. In this thesis, we routinely use the the Quasi-3D approach, consisting of the 2D spectral/*hp* elements with 1D Fourier expansions are used to discretise the cross stream plane and streamwise flow respectively. The velocity and pressure in the spectral/*hp* plane is described by two dimensional modified bases with Fourier

expansions,

$$\begin{bmatrix} \mathbf{u}^{\delta}(x,y,z,t) \\ p^{\delta}(x,y,z,t) \end{bmatrix} = \sum_{k=0}^{N_z-1} \sum_{p=0}^{P} \sum_{q=0}^{P} \psi_p(x)\psi_q(y)e^{ik\beta z} \begin{bmatrix} \hat{\mathbf{u}}_{p,q,k}(t) \\ \hat{p}_{p,q,k}(t) \end{bmatrix} = \sum_{k=0}^{N-1} e^{ik\beta z} \begin{bmatrix} \tilde{\mathbf{u}}_k(x,y,t) \\ \tilde{p}_k(x,y,t) \end{bmatrix} \tag{2.62}$$

where $\beta = \frac{2\pi}{L_z}$ is the spanwise wavenumber, L_z the spanwise length, N_z the number of Fourier expansions. Substituting equation 2.62 into the Navier-Stokes equations and taking the Fourier transform (equivalently to the Galerkin projection with respect to Fourier expansion as a test function) yields a system of N_z decoupled equations, amenable for parallel processing,

$$\frac{\partial \tilde{\mathbf{u}}_k}{\partial t} = -\tilde{\nabla}_k \tilde{p}_k + \nu(\nabla^2_{x,y} - k^2\beta^2)\tilde{\mathbf{u}}_k - \widehat{[(\mathbf{u}\cdot\nabla)\mathbf{u}]}_k \tag{2.63a}$$

$$-k\beta\tilde{\nabla}\cdot\tilde{\mathbf{u}}_k = 0, \quad k = 0, ..., N_z - 1 \tag{2.63b}$$

where, $\tilde{\nabla}_k = (\frac{\partial}{\partial x}, \frac{\partial}{\partial y}, ik\beta)$, $\nabla^2_{x,y} = (\frac{\partial^2}{\partial x^2}, \frac{\partial^2}{\partial y^2})$ and $\widehat{[(\mathbf{u}\cdot\nabla)\mathbf{u}]}_k$ refers to the Fourier-transformed of the k^{th} nonlinear term.

2.4.3 Enforcing constant flow rate

Due to the enforced periodicity in the streamwise z direction via Fourier expansions, a pressure drop cannot be prescribed to drive the flow for $Re > 0$ scenarios. To sustain the flow, we use a Green's function approach [**?**] to impose a constant flow rate,

$$W_b = Q(\mathbf{u}) = \frac{1}{2L_x h}\int_{x,y} \mathbf{u}\, \mathrm{d}x\mathrm{d}z, \tag{2.64}$$

where W_b and $Q(\cdot)$ refer to the desired flow rate and flow rate operator. A correction velocity, $\mathbf{u}_{corr}$, is obtained by solving the linear Stokes equation with unit forcing once and is stored for reuse. At the end of every time-step, the final velocity field, $\mathbf{u}$, is then updated by adding this correction velocity to the homogeneous velocity obtained from the velocity correction scheme,

$$\mathbf{u} = \mathbf{u}_h + \gamma\mathbf{u}_{corr}, \tag{2.65}$$

where γ defined as,

$$\gamma = \frac{W_b - Q(\mathbf{u}_h)}{Q(\mathbf{u}_{corr})}, \tag{2.66}$$

is adjusted to satisfy the desired flow rate, W_b. The flow rate, W_b, is related to the laminar centreline velocity $W_c = 3/2W_b$, which defines the Reynolds number, $Re = W_c h/\nu$. For more details on the numerical method, the reader is referred to **?**.

2.5 Stability analysis of the Navier-Stokes equations

2.5.1 Linear Stability analysis

Linear stability analysis concerns the study of the evolution of small perturbations around a base flow. To study the dynamics of infinitetisimal perturbations about a base flow, the time evolution equation for the perturbations dynamics typically reduces to,

$$\frac{\partial}{\partial t}\mathbf{u}' = \mathbf{L}\mathbf{u}', \tag{2.67}$$

where $\mathbf{L}, \mathbf{u}$ refers to the linearised operator and a vector of velocity perturbations. In this case, the linear operator is the linearised Navier Stokes equation which has the form,

$$\mathbf{L} = \begin{bmatrix} -(\mathbf{U}\cdot\nabla) - (\nabla\mathbf{U})\cdot + \frac{1}{Re}\nabla^2 & -\nabla \\ \nabla\cdot & 0 \end{bmatrix}, \tag{2.68}$$

where $\mathbf{U}$ is referred to as the base flow, where the linear operator $\mathbf{L} \in \mathbf{R}^{N_g, N_g}$, N_g refers to the number of global degrees of freedom. For a given initial condition, $\mathbf{u}'(\mathbf{x}, t = 0) = \mathbf{u}_0$, the evolution of velocity perturbation up to time T is therefore,

$$\mathbf{u}(\mathbf{x}', t) = \mathcal{A}(T, Re)\mathbf{u}_0 \tag{2.69}$$

where $\mathcal{A}(T, Re) = \exp(\mathbf{L}T)$ refers to the linear evolution operator that propagates perturbations to $t = T$. Suppose that the perturbation velocities can be represented by eigenmode solutions,

$$\mathbf{u}'(\mathbf{x}, t) = \tilde{\mathbf{u}}(\mathbf{x})\exp(\lambda t) + \text{c.c} \tag{2.70}$$

where $\lambda_j, \tilde{\mathbf{u}}_j$ refer to the j^{th} eigenvalue and eigenmode which can becomplex, and c.c refers to the complex conjugate. Substituting the ansatz above, we get an eigenvalue problem of

$$\mathcal{A}(T, Re)\tilde{\mathbf{u}}_j = \mu_j\tilde{\mathbf{u}}_j, \quad \mu_j = \exp(\lambda_j T). \tag{2.71}$$

For steady base flows, we are primarily interested in λ_j instead of μ_j, and T is chosen to be one [Barkley et al., 2008]. In choosing T, one has be careful not to choose a value larger than the period of the leading eigenvalue in order to avoid aliasing issues. For periodic base flows, μ_j is referred to the Floquet multiplier. If $|\lambda_j| > 1$, then infinitisimal perturbations grow exponentially and the fluid system is recognised as being linearly unstable. For $|\lambda_j| < 0$, infinitisimal perturbations will decay exponentially and the fluid system if linearly stable. If $|\lambda| = 0$, it indicates a bifurcation point. Matrix $\mathcal{A}(T, Re)$ is considered sufficiently large that direct diagonalisation using the QR algorithm where the operation count is of $O(N_g^3)$ becomes infeasible. Furthermore, A is not directly available in the splitting code. Instead, perform the computating in a matrix-free way, where we act matrix $\mathcal{A}$ with some arbitrary vector $\mathbf{u}_0$ iteratively [Tuckerman and Barkley, 2000]. By applying matrix $\mathcal{A}$ to $\mathbf{u}_0$ n times, we generate a sequence of of vectors give as $\mathbf{u}_n = \mathcal{A}^n\mathbf{u}_0$ which approaches the dominant

eigenvector, corresponding to the largest magnitude where the Rayleigh quotients $h_n = \mathbf{u}_n^T \mathcal{A}\mathbf{u}_n / \mathbf{u}_n^T \mathbf{u}$ converges to the eigenvalue. This idea of the time-stepper approach to compute the eigenvalues is that minimal modifications are required to be made to an existing unsteady code. However, this idea only computes the dominant eigenmode, and in practice we desire 2-4 eigenpairs, and require perhaps 4-8 eigenpairs to serve as an 'error-absorbing' buffer. The calculation of several pairs is known as the Arnoldi methods, which is related to the generalisation of the power method, ultilised in this thesis. In this method, we generate a sequence of vectors $\mathbf{T}_k$ of normalised vectors are generated such that.

$$\mathbf{T}_k = [\mathbf{u}_0, \mathbf{u}_1, ..., \mathbf{u}_{k-1}] = \left[\mathbf{u}_0, \frac{\mathcal{A}(T, Re)\mathbf{u}_0}{\alpha_1}, \frac{\mathcal{A}(T, Re)\mathbf{u}_1}{\alpha_2}, ..., \frac{\mathcal{A}(T, Re)\mathbf{u}_{k-1}}{\alpha_k}\right], \tag{2.72}$$

where α_j is a factor chosen such that $||\mathbf{u}_j|| = 1$ has unit-norm and the span of $\mathbf{T}_k$ span the *Krylov subspace*, where k refers to the number of eigenpairs sough after. Then, an iterative QR decomposition of the Krylove subspace is performed,

$$\mathbf{K}_k \mathbf{V}_k = \mathbf{V}_k \mathbf{H}_k, \tag{2.73}$$

where $\mathbf{H} \in \mathbf{R}^{k,k}, \mathbf{V} \in \mathbf{R}^{N_g,k}$ refers to the Hessenberg matrix and an upper triangular matrix. The eigenvalues of $\mathcal{A}$ is approximated by the eigenvalues of $\mathbf{H}$, and its eigenvectors multiplied by $\mathbf{V}$ approximate the eigenvectors of $\mathcal{A}$ [similarity transform..]. We note that the solving the eigenvalue problem of $\mathbf{H} \in \mathbf{R}^{k,k}$ is much cheaper than $\mathcal{A} \in \mathbf{R}^{N_g,N_g}$. We also note that since $\mathcal{A} = \exp(\mathbf{L}t)$, this method if referred to the exponential power method, where the dominant eigenvector of $\mathcal{A}$ is the eigenvalue of $\mathcal{L}$ with the largest real part.

Maths

Theorem 1 (Krylov Subspaces)**.** Given a matrix $\mathbf{A} \in \mathbb{R}^{n\times n}$ and a non-zero vector $\mathbf{x}_0 \in \mathbb{R}^n$, the k^{th}-Krylov subspace, $\mathcal{K}_n(\mathbf{A}, \mathbf{x}_0, k)$ is generated by,

$$\mathcal{K}_n(\mathbf{A}, \mathbf{x}_0, k) = \text{span}\{\mathbf{x}_0, \mathbf{A}\mathbf{x}_0, \mathbf{A}^2\mathbf{x}_0, \mathbf{A}^3\mathbf{x}_0, ..., \mathbf{A}^{k-1}\mathbf{x}_0\}. \tag{2.74}$$

By using the span of the k^{th}-Krylov subspace, we can approximate matrix $\mathcal{A}$ by an upper Hessenberg matrix, $\mathbf{H}$, (all entries below the first subdiagonal are zero) using the Hessenberg reduction,

Theorem 2. Hessenberg reduction Given a matrix $\mathbf{A} \in \mathbb{R}^{n\times n}$, there exists an orthogonal matrix $\mathbf{Q} \in \mathbb{R}^{n\times n}$ and a Hessenberg matrix $\mathbf{H} \in \mathbb{R}^{n\times n}$ such that

$$\mathbf{A} = \mathbf{Q}\mathbf{H}\mathbf{Q}^T \tag{2.75}$$

Since matrices $\mathbf{A}$ and $\mathbf{H}$ are similar matrices by definition, then their eigenvalues are similar, $\lambda\mathbf{A} = \lambda\mathbf{H}$. In practice, we do not compute $\mathbf{H}$ in full. Instead, we construct k-columns of matrix $\mathbf{Q}$ by considering an orthornomal set of k vectors, $\mathbf{q}_0, \mathbf{q}_1, ..., \mathbf{q}_{k-1}$ from the k-Krylov subspace, $\mathcal{K}_n(\mathbf{A}, \mathbf{x}_0, k)$,

$$\text{span}\{\mathbf{q}_0, \mathbf{q}_1, ..., \mathbf{q}_{k-1}\} = \text{span}\{\mathbf{x}_0, \mathbf{A}\mathbf{x}_0, ..., \mathbf{A}^{k-1}\mathbf{x}_0\} \tag{2.76}$$

The orthornomal vectors $\mathbf{Q}$ is generated by performing a Gram-schmidt orthogonalisation The power method is defined as,

Theorem 3 (Power method)**.** If $\mathbf{A} \in \mathbb{R}^{n\times n}$ is a diagonalisable, then there is a non-zero vector, $\mathbf{u}_0$ such that the sequence of vector given by,

(2.77)

approaches the dominant of eigenvector of $\mathbf{A}$.

Let λ_i be the eigenvalues of a matrix $\mathbf{A} \in \mathbb{R}^{n\times n}$. λ_1 is called the dominant eigenvalue of $\mathbf{A}$ if,

$$|\lambda_1| > |\lambda_i|, \quad i = 2, ..., n \tag{2.78}$$

The eigenvector corresponding to λ_1 is called the dominant eigenvector of $\mathbf{A}$.

2.5.2 Edge tracking

In the section, we consider the dynamical system interpretation of transition, where the laminar state is separated by the turbulent state by an edge, referred to the edge of chaos. Along this edge, there could be attractors, sometimes in the form of travelling-waves, tori, and high-order invariant sets, known as the edge states. For the edge tracking, we use the bisection method [Skufca et al., 2006, Schneider et al., 2007, Khapko et al., 2016], with an initial condition given by

$$\mathbf{x}_0 = \chi \mathbf{x}_L + (1 - \chi)\mathbf{x}_T \tag{2.79}$$

where $\mathbf{x}_0$ refers to an initial condition consisting of a weighted sum, $\chi \in [0, 1]$, between a laminar state, $\mathbf{x}_l$, and a turbulent state, $\mathbf{x}_T$. Since the laminar and turbulent state forms a bistable system, there could be (at least) one critical value of $\chi \in [0, 1]$, where the trajectory walks along the 'edge' between the turbulent and laminar state without decaying to either states. To find this χ_c, we perform n successive bisections between χ_L^n, χ_T^n, the upper and lower bounds such that the trajectory relaminarises or become turbulent respectively, where χ^n is updated by $\chi^n = \frac{1}{2}(\chi_L^n + \chi_T^n)$ At every n^{th} bisection, it involves a stopping criteria, a tolerance based on the deviation of an observable (e.g. wall shear stresses) away from the initial condition. Then, a direct numerical simulation is reinitialised with an initial condition given by equation (2.79) For every successive bisection, the difference between two trajectories, $\Delta\chi^n = \chi_L^n - \chi_T^n$, decays like $\Delta\chi^n \sim 0.5^n$, and is related to the Lyapunov exponent of the edge

$$\Delta\chi \approx C \exp(\mu_e t) \tag{2.80}$$

where μ_e, C refers to the Lyapunov exponent of the edge and a constant. In practice, we consider $n = 10, 20$ and for $n = 10$, the solution along the edge is converged. After we determine the critical χ_c, we repeat the bisections step by replacing the laminar state, $\mathbf{x}_L$, and the turbulent state $\mathbf{x}_T$, which the solution trajectory with χ_L and χ_T, that has been terminated after exceeded the threshold. We refer this repetition as the number of 'outer' bisections, while the bisection for χ^n is referred to 'inner bisections' After a certain number of 'outer' bisections, the trajectory may converge towards

an attractor, which may exist in a from of travelling-waves, periodic orbits or a chaotic attractor. This attractor sits along the edge is referred to as the edge state, a saddle acting as a separatrix between the turbulent and laminar attractor. We describe the algorithm of edge tracking in algorithm 2.5.2

Algorithm 1 Algorithm for edge tracking between a turbulent and laminar state

Initialise `maxInBisects, maxOutBisects` ▷ Maximum inner and outer bisections
Initialise `tol` ▷ Tolerance for stopping criteria (e.g., wall-shear stress)
`outBisects` $\leftarrow 0$
while `outBisects` < `maxOutBisects` **do**
    if `outBisects` == 0 **then**
        $\mathbf{x}_L, \mathbf{x}_T \leftarrow$ `input()` ▷ Initial laminar and turbulent states
    end if
    $\chi_L \leftarrow 0,\ \chi_T \leftarrow 1,\ \chi \leftarrow \frac{1}{2}(\chi_L + \chi_T)$ ▷ Initialise bisection coefficients
    $\mathbf{x}_0 \leftarrow \chi \mathbf{x}_T + (1-\chi)\mathbf{x}_L$ ▷ Initialise initial condition
    `inBisects` $\leftarrow 0$
    while `inBisects` < `maxInBisects` **do**
        $\mathbf{k} \leftarrow 0, \Delta \leftarrow 10^6$
        while $\Delta >$ `tol` **do**
            $\mathbf{x}_{k+1} \leftarrow$ `TimeIntegrate`$(\mathbf{x}_k)$
            $\Delta \leftarrow |\mathbf{x}_{k+1} - \mathbf{x}_0|$ ▷ Deviation from initial condition
            $\mathbf{k} \leftarrow \mathbf{k} + 1$
        end while
        if `isTurbulent`$(\mathbf{x}_k)$ **then** ▷ Check if terminal state is turbulent
            $\chi_L \leftarrow \chi$ ▷ $\mathbf{x}_L$ gets larger weight
            if `inBisects` == `maxInBisects` - 1 **then**
                $\mathbf{x}_T \leftarrow \mathbf{x}_k$ ▷ Save turbulent-leaning initial condition
                `break`
            end if
        else
            $\chi_T \leftarrow \chi$
            if `inBisects` == `maxInBisects` - 1 **then**
                $\mathbf{x}_L \leftarrow \mathbf{x}_k$ ▷ Save laminar-leaning initial condition
                `break`
            end if
        end if
        $\chi \leftarrow \frac{1}{2}(\chi_L + \chi_T)$
        $\mathbf{x}_0 \leftarrow \chi \mathbf{x}_L + (1-\chi)\mathbf{x}_T$ ▷ Update initial conditions
        `inBisects++`
    end while
    `outBisects++`
end while

Bibliography

Clouds streets and comma clouds near svalbard. https://earthobservatory.nasa.gov/images/87749/clouds-streets-and-comma-clouds-near-svalbard.

H. Affan and R. Friedrich. Spiral defect chaos in an advection-reaction-diffusion system. *Physical Review E*, 89(6):062920, June 2014. ISSN 1539-3755, 1550-2376. doi: 10.1103/PhysRevE.89.062920. URL https://link.aps.org/doi/10.1103/PhysRevE.89.062920.

Guenter Ahlers. Experiments on spatio-temporal chaos.

Mitsunobu Akiyama, Guang-Jyh Hwang, and KC Cheng. Experiments on the onset of longitudinal vortices in laminar forced convection between horizontal plates. 1971. ISSN 0022-1481.

Kerstin Avila, David Moxey, Alberto De Lozar, Marc Avila, Dwight Barkley, and Björn Hof. The Onset of Turbulence in Pipe Flow. *Science*, 333(6039):192–196, July 2011. ISSN 0036-8075, 1095-9203. doi: 10.1126/science.1203223. URL https://www.science.org/doi/10.1126/science.1203223.

Marc Avila, Ashley P. Willis, and Björn Hof. On the transient nature of localized pipe flow turbulence. *Journal of Fluid Mechanics*, 646:127–136, March 2010. ISSN 0022-1120, 1469-7645. doi: 10.1017/S0022112009993296. URL https://www.cambridge.org/core/product/identifier/S0022112009993296/type/journal_article.

Marc Avila, Dwight Barkley, and Björn Hof. Transition to Turbulence in Pipe Flow. *Annual Review of Fluid Mechanics*, 55(1):575–602, January 2023. ISSN 0066-4189, 1545-4479. doi: 10.1146/annurev-fluid-120720-025957. URL https://www.annualreviews.org/doi/10.1146/annurev-fluid-120720-025957.

Kapil M. S. Bajaj, David S. Cannell, and Guenter Ahlers. Competition between spiral-defect chaos and rolls in Rayleigh-Bénard convection. *Physical Review E*, 55(5):R4869–R4872, May 1997. ISSN 1063-651X, 1095-3787. doi: 10.1103/PhysRevE.55.R4869. URL https://link.aps.org/doi/10.1103/PhysRevE.55.R4869.

D. Barkley, H. M. Blackburn, and S. J. Sherwin. Direct optimal growth analysis for timesteppers. *International Journal for Numerical Methods in Fluids*, 57(9):1435–1458, July 2008. ISSN 0271-2091, 1097-0363. doi: 10.1002/fld.1824. URL https://onlinelibrary.wiley.com/doi/10.1002/fld.1824.

Dwight Barkley and Laurette S. Tuckerman. Computational Study of Turbulent Laminar Patterns in Couette Flow. *Physical Review Letters*, 94(1):014502, January 2005. doi: 10.1103/PhysRevLett.94.014502. URL https://link.aps.org/doi/10.1103/PhysRevLett.94.014502. Publisher: American Physical Society.

Dwight Barkley and Laurette S Tuckerman. Mean flow of turbulent–laminar patterns in plane Couette flow. *Journal of Fluid Mechanics*, 576:109–137, 2007. ISSN 1469-7645. Publisher: Cambridge University Press.

Myron J. Block. Surface Tension as the Cause of Bénard Cells and Surface Deformation in a Liquid Film. *Nature*, 178(4534):650–651, September 1956. ISSN 0028-0836, 1476-4687. doi: 10.1038/178650a0. URL https://www.nature.com/articles/178650a0.

Eberhard Bodenschatz, David S. Cannell, John R. De Bruyn, Robert Ecke, Yu-Chou Hu, Kristina Lerman, and Guenter Ahlers. Experiments on three systems with non-variational aspects. *Physica D: Nonlinear Phenomena*, 61(1-4):77–93, December 1992. ISSN 01672789. doi: 10.1016/0167-2789(92)90150-L. URL https://linkinghub.elsevier.com/retrieve/pii/016727899290150L.

Eberhard Bodenschatz, Werner Pesch, and Guenter Ahlers. Recent Developments in Rayleigh-Bénard Convection. *Annual Review of Fluid Mechanics*, 32(1):709–778, January 2000. ISSN 0066-4189, 1545-4479. doi: 10.1146/annurev.fluid.32.1.709. URL https://www.annualreviews.org/doi/10.1146/annurev.fluid.32.1.709.

Katarzyna Borońska and Laurette S. Tuckerman. Extreme multiplicity in cylindrical Rayleigh-Bénard convection. I. Time dependence and oscillations. *Physical Review E*, 81(3):036320, March 2010a. ISSN 1539-3755, 1550-2376. doi: 10.1103/PhysRevE.81.036320. URL https://link.aps.org/doi/10.1103/PhysRevE.81.036320.

Katarzyna Borońska and Laurette S. Tuckerman. Extreme multiplicity in cylindrical Rayleigh-Bénard convection. II. Bifurcation diagram and symmetry classification. *Physical Review E*, 81(3):036321, March 2010b. ISSN 1539-3755, 1550-2376. doi: 10.1103/PhysRevE.81.036321. URL https://link.aps.org/doi/10.1103/PhysRevE.81.036321.

N. Boullé, V. Dallas, and P. E. Farrell. Bifurcation analysis of two-dimensional Rayleigh-Bénard convection using deflation. *Physical Review E*, 105(5):055106, May 2022. ISSN 2470-0045, 2470-0053. doi: 10.1103/PhysRevE.105.055106. URL https://link.aps.org/doi/10.1103/PhysRevE.105.055106.

Luca Brandt. The lift-up effect: The linear mechanism behind transition and turbulence in shear flows. *European Journal of Mechanics - B/Fluids*, 47:80–96, September 2014. ISSN 09977546. doi: 10.1016/j.euromechflu.2014.03.005. URL https://linkinghub.elsevier.com/retrieve/pii/S0997754614000405.

F. H. Busse. The oscillatory instability of convection rolls in a low Prandtl number fluid. *Journal of Fluid Mechanics*, 52(1):97–112, March 1972. ISSN 0022-1120, 1469-7645. doi: 10.1017/S0022112072002988. URL https://www.cambridge.org/core/product/identifier/S0022112072002988/type/journal_article.

F H Busse. Non-linear properties of thermal convection. *Reports on Progress in Physics*, 41(12): 1929–1967, December 1978. ISSN 0034-4885, 1361-6633. doi: 10.1088/0034-4885/41/12/003. URL https://iopscience.iop.org/article/10.1088/0034-4885/41/12/003.

F. H. Busse and J. A. Whitehead. Instabilities of convection rolls in a high Prandtl number fluid. *Journal of Fluid Mechanics*, 47(2):305–320, May 1971. ISSN 0022-1120, 1469-7645. doi: 10.1017/S0022112071001071. URL https://www.cambridge.org/core/product/identifier/S0022112071001071/type/journal_article.

Kathryn M. Butler and Brian F. Farrell. Three-dimensional optimal perturbations in viscous shear flow. *Physics of Fluids A: Fluid Dynamics*, 4(8):1637–1650, August 1992. ISSN 0899-8213. doi: 10.1063/1.858386. URL https://pubs.aip.org/pof/article/4/8/1637/402702/Three-dimensional-optimal-perturbations-in-viscous.

Henri Bénard. Les tourbillons cellulaires dans une nappe liquide. - Méthodes optiques d'observation et d'enregistrement. *Journal de Physique Théorique et Appliquée*, 10(1):254–266, 1901. ISSN 0368-3893. doi: 10.1051/jphystap:0190100100025400. URL http://www.edpsciences.org/10.1051/jphystap:0190100100025400.

Reha V. Cakmur, David A. Egolf, Brendan B. Plapp, and Eberhard Bodenschatz. Bistability and Competition of Spatiotemporal Chaotic and Fixed Point Attractors in Rayleigh-Bénard Convection. *Physical Review Letters*, 79(10):1853–1856, September 1997a. ISSN 0031-9007, 1079-7114. doi: 10.1103/PhysRevLett.79.1853. URL https://link.aps.org/doi/10.1103/PhysRevLett.79.1853.

Reha V. Cakmur, David A. Egolf, Brendan B. Plapp, and Eberhard Bodenschatz. Transition from Spatiotemporal Chaos to Ideal Straight Rolls in Rayleigh-Benard Convection, February 1997b. URL http://arxiv.org/abs/patt-sol/9702003. arXiv:patt-sol/9702003.

Philippe Carrière and Peter A. Monkewitz. Convective versus absolute instability in mixed Rayleigh–Bénard–Poiseuille convection. *Journal of Fluid Mechanics*, 384:243–262, April 1999. ISSN 0022-1120, 1469-7645. doi: 10.1017/S0022112098004145. URL https://www.cambridge.org/core/product/identifier/S0022112098004145/type/journal_article.

K.-H. Chiam, M. R. Paul, M. C. Cross, and H. S. Greenside. Mean flow and spiral defect chaos in Rayleigh-Bénard convection. *Physical Review E*, 67(5):056206, May 2003. ISSN 1063-651X, 1095-3787. doi: 10.1103/PhysRevE.67.056206. URL https://link.aps.org/doi/10.1103/PhysRevE.67.056206.

R. M. Clever and F. H. Busse. Instabilities of longitudinal rolls in the presence of Poiseuille flow. *Journal of Fluid Mechanics*, 229(-1):517, August 1991. ISSN 0022-1120, 1469-7645. doi: 10.1017/S0022112091003142. URL http://www.journals.cambridge.org/abstract_S0022112091003142.

A. Cloot and G. Lebon. A nonlinear stability analysis of the Bénard–Marangoni problem. *Journal of Fluid Mechanics*, 145(-1):447, August 1984. ISSN 0022-1120, 1469-7645. doi: 10.1017/S0022112084003013. URL http://www.journals.cambridge.org/abstract_S0022112084003013.

Vincent Croquette. Convective pattern dynamics at low Prandtl number: Part I. *Contemporary Physics*, 30(2):113–133, March 1989a. ISSN 0010-7514, 1366-5812. doi: 10.1080/00107518908225511. URL http://www.tandfonline.com/doi/abs/10.1080/00107518908225511.

Vincent Croquette. Convective pattern dynamics at low Prandtl number: Part II. *Contemporary Physics*, 30(3):153–171, May 1989b. ISSN 0010-7514, 1366-5812. doi: 10.1080/00107518908222594. URL http://www.tandfonline.com/doi/abs/10.1080/00107518908222594.

W. Decker, W. Pesch, and A. Weber. Spiral defect chaos in Rayleigh-Bénard convection. *Physical Review Letters*, 73(5):648–651, August 1994. ISSN 0031-9007. doi: 10.1103/PhysRevLett.73.648. URL https://link.aps.org/doi/10.1103/PhysRevLett.73.648.

Lifang Dong, Fucheng Liu, Shuhua Liu, Yafeng He, and Weili Fan. Observation of spiral pattern and spiral defect chaos in dielectric barrier discharge in argon/air at atmospheric pressure. *Physical Review E*, 72(4):046215, October 2005. ISSN 1539-3755, 1550-2376. doi: 10.1103/PhysRevE.72.046215. URL https://link.aps.org/doi/10.1103/PhysRevE.72.046215.

Y. Duguet, P. Schlatter, and D. S. Henningson. Formation of turbulent patterns near the onset of transition in plane Couette flow. *Journal of Fluid Mechanics*, 650:119–129, May 2010. ISSN 0022-1120, 1469-7645. doi: 10.1017/S0022112010000297. URL https://www.cambridge.org/core/product/identifier/S0022112010000297/type/journal_article.

Robert E. Ecke, Yuchou Hu, Ronnie Mainieri, and Guenter Ahlers. Excitation of Spirals and Chiral Symmetry Breaking in Rayleigh-Bénard Convection. *Science*, 269(5231):1704–1707, September 1995. ISSN 0036-8075, 1095-9203. doi: 10.1126/science.269.5231.1704. URL https://www.science.org/doi/10.1126/science.269.5231.1704.

Wiktor Eckhaus. *Studies in Non-Linear Stability Theory*, volume 6 of *Springer Tracts in Natural Philosophy*. Springer Berlin Heidelberg, Berlin, Heidelberg, 1965. ISBN 978-3-642-88319-4 978-3-642-88317-0. doi: 10.1007/978-3-642-88317-0. URL http://link.springer.com/10.1007/978-3-642-88317-0.

David A. Egolf, Ilarion V. Melnikov, and Eberhard Bodenschatz. Importance of Local Pattern Properties in Spiral Defect Chaos. *Physical Review Letters*, 80(15):3228–3231, April 1998. ISSN

0031-9007, 1079-7114. doi: 10.1103/PhysRevLett.80.3228. URL https://link.aps.org/doi/10.1103/PhysRevLett.80.3228.

David A. Egolf, Ilarion V. Melnikov, Werner Pesch, and Robert E. Ecke. Mechanisms of extensive spatiotemporal chaos in Rayleigh–Bénard convection. *Nature*, 404(6779):733–736, April 2000. ISSN 0028-0836, 1476-4687. doi: 10.1038/35008013. URL https://www.nature.com/articles/35008013.

T. Ellingsen and E. Palm. Stability of linear flow. *The Physics of Fluids*, 18(4):487–488, April 1975. ISSN 0031-9171. doi: 10.1063/1.861156. URL https://pubs.aip.org/pfl/article/18/4/487/459138/Stability-of-linear-flow.

Greg Evans and Ralph Greif. Unsteady three-dimensional mixed convection in a heated horizontal channel with applications to chemical vapor deposition. *International Journal of Heat and Mass Transfer*, 34(8):2039–2051, August 1991. ISSN 00179310. doi: 10.1016/0017-9310(91)90215-Z. URL https://linkinghub.elsevier.com/retrieve/pii/001793109190215Z.

Brian F. Farrell. Optimal excitation of perturbations in viscous shear flow. *The Physics of Fluids*, 31(8):2093–2102, August 1988. ISSN 0031-9171. doi: 10.1063/1.866609. URL https://pubs.aip.org/pfl/article/31/8/2093/966463/Optimal-excitation-of-perturbations-in-viscous.

Keisuke Fukui, Masamoto Nakajima, and Hiromasa Ueda. The longitudinal vortex and its effects on the transport processes in combined free and forced laminar convection between horizontal and inclined parallel plates. *International Journal of Heat and Mass Transfer*, 26(1):109–120, January 1983. ISSN 00179310. doi: 10.1016/S0017-9310(83)80013-1. URL https://linkinghub.elsevier.com/retrieve/pii/S0017931083800131.

K. S. Gage and W. H. Reid. The stability of thermally stratified plane Poiseuille flow. *Journal of Fluid Mechanics*, 33(1):21–32, July 1968. ISSN 0022-1120, 1469-7645. doi: 10.1017/S0022112068002326. URL https://www.cambridge.org/core/product/identifier/S0022112068002326/type/journal_article.

J. F. Gibson, J. Halcrow, and P. Cvitanović. Visualizing the geometry of state space in plane Couette flow. *Journal of Fluid Mechanics*, 611:107–130, September 2008. ISSN 0022-1120, 1469-7645. doi: 10.1017/S002211200800267X. URL https://www.cambridge.org/core/product/identifier/S002211200800267X/type/journal_article.

J. F. Gibson, J. Halcrow, and P. Cvitanović. Equilibrium and travelling-wave solutions of plane Couette flow. *Journal of Fluid Mechanics*, 638:243–266, November 2009. ISSN 0022-1120, 1469-7645. doi: 10.1017/S0022112009990863. URL https://www.cambridge.org/core/product/identifier/S0022112009990863/type/journal_article.

Sébastien Gomé, Laurette S. Tuckerman, and Dwight Barkley. Statistical transition to turbulence in plane channel flow. *Physical Review Fluids*, 5(8):083905, August 2020. ISSN 2469-990X. doi: 10.1103/PhysRevFluids.5.083905. URL https://link.aps.org/doi/10.1103/PhysRevFluids.5.083905.

Michael D. Graham and Daniel Floryan. Exact Coherent States and the Nonlinear Dynamics of Wall-Bounded Turbulent Flows. *Annual Review of Fluid Mechanics*, 53(1):227–253, January 2021. ISSN 0066-4189, 1545-4479. doi: 10.1146/annurev-fluid-051820-020223. URL https://www.annualreviews.org/doi/10.1146/annurev-fluid-051820-020223.

J. Halcrow, J. F. Gibson, P. Cvitanović, and D. Viswanath. Heteroclinic connections in plane Couette flow. *Journal of Fluid Mechanics*, 621:365–376, February 2009. ISSN 0022-1120, 1469-7645. doi: 10.1017/S0022112008005065. URL https://www.cambridge.org/core/product/identifier/S0022112008005065/type/journal_article.

James M. Hamilton, John Kim, and Fabian Waleffe. Regeneration mechanisms of near-wall turbulence structures. *Journal of Fluid Mechanics*, 287:317–348, March 1995. ISSN 0022-1120, 1469-7645. doi: 10.1017/S0022112095000978. URL https://www.cambridge.org/core/product/identifier/S0022112095000978/type/journal_article.

C.Q Hoard, C.R Robertson, and A Acrivos. Experiments on the cellular structure in bénard convection. *International Journal of Heat and Mass Transfer*, 13(5):849–856, May 1970. ISSN 00179310. doi: 10.1016/0017-9310(70)90130-4. URL https://linkinghub.elsevier.com/retrieve/pii/0017931070901304.

B. Hof, P. G. J. Lucas, and T. Mullin. Flow state multiplicity in convection. *Physics of Fluids*, 11(10):2815–2817, October 1999. ISSN 1070-6631, 1089-7666. doi: 10.1063/1.870178. URL https://pubs.aip.org/pof/article/11/10/2815/254396/Flow-state-multiplicity-in-convection.

M. Z. Hossain and J. M. Floryan. Drag reduction in a thermally modulated channel. *Journal of Fluid Mechanics*, 791:122–153, March 2016. ISSN 0022-1120, 1469-7645. doi: 10.1017/jfm.2016.42. URL https://www.cambridge.org/core/product/identifier/S0022112016000422/type/journal_article.

M. Z. Hossain and J. M. Floryan. On the role of surface grooves in the reduction of pressure losses in heated channels. *Physics of Fluids*, 32(8):083610, August 2020. ISSN 1070-6631, 1089-7666. doi: 10.1063/5.0018416. URL https://pubs.aip.org/pof/article/32/8/083610/1060903/On-the-role-of-surface-grooves-in-the-reduction-of.

M. Z. Hossain, D. Floryan, and J. M. Floryan. Drag reduction due to spatial thermal modulations. *Journal of Fluid Mechanics*, 713:398–419, December 2012. ISSN 0022-1120, 1469-7645. doi: 10.1017/jfm.2012.465. URL https://www.cambridge.org/core/product/identifier/S002211201200465X/type/journal_article.

Yuchou Hu, Robert Ecke, and Guenter Ahlers. Convection near threshold for Prandtl numbers near 1. *Physical Review E*, 48(6):4399–4413, December 1993. ISSN 1063-651X, 1095-3787. doi: 10.1103/PhysRevE.48.4399. URL https://link.aps.org/doi/10.1103/PhysRevE.48.4399.

Yuchou Hu, Robert Ecke, and Guenter Ahlers. Convection for Prandtl numbers near 1: Dynamics of textured patterns. *Physical Review E*, 51(4):3263–3279, April 1995. ISSN 1063-651X, 1095-3787. doi: 10.1103/PhysRevE.51.3263. URL https://link.aps.org/doi/10.1103/PhysRevE.51.3263.

Yuchou Hu, Robert E. Ecke, and Guenter Ahlers. Convection under rotation for Prandtl numbers near 1: Linear stability, wave-number selection, and pattern dynamics. *Physical Review E*, 55(6):6928–6949, June 1997. ISSN 1063-651X, 1095-3787. doi: 10.1103/PhysRevE.55.6928. URL https://link.aps.org/doi/10.1103/PhysRevE.55.6928.

Harold Jeffreys. Some cases of instability in fluid motion. *Proceedings of the Royal Society of London. Series A, Containing Papers of a Mathematical and Physical Character*, 118(779):195–208, March 1928. ISSN 0950-1207, 2053-9150. doi: 10.1098/rspa.1928.0045. URL https://royalsocietypublishing.org/doi/10.1098/rspa.1928.0045.

Klavs F. Jensen, Erik O. Einset, and Dimitrios I. Fotiadis. Flow Phenomena in Chemical Vapor Deposition of Thin Films. *Annual Review of Fluid Mechanics*, 23(1):197–232, January 1991. ISSN 0066-4189, 1545-4479. doi: 10.1146/annurev.fl.23.010191.001213. URL https://www.annualreviews.org/doi/10.1146/annurev.fl.23.010191.001213.

J. John Soundar Jerome, Jean-Marc Chomaz, and Patrick Huerre. Transient growth in Rayleigh-Bénard-Poiseuille/Couette convection. *Physics of Fluids*, 24(4):044103, April 2012. ISSN 1070-6631, 1089-7666. doi: 10.1063/1.4704642. URL https://pubs.aip.org/pof/article/24/4/044103/257562/Transient-growth-in-Rayleigh-Benard-Poiseuille.

A. Karimi, Zhi-Feng Huang, and M. R. Paul. Exploring spiral defect chaos in generalized Swift-Hohenberg models with mean flow. *Physical Review E*, 84(4):046215, October 2011. ISSN 1539-3755, 1550-2376. doi: 10.1103/PhysRevE.84.046215. URL https://link.aps.org/doi/10.1103/PhysRevE.84.046215.

George Karniadakis and Spencer J Sherwin. *Spectral/hp element methods for computational fluid dynamics*. Oxford University Press, 2005. ISBN 0-19-852869-8.

George Em Karniadakis, Moshe Israeli, and Steven A Orszag. High-order splitting methods for the incompressible Navier-Stokes equations. *Journal of Computational Physics*, 97(2):414–443, December 1991. ISSN 00219991. doi: 10.1016/0021-9991(91)90007-8. URL https://linkinghub.elsevier.com/retrieve/pii/0021999191900078.

Genta Kawahara and Shigeo Kida. Periodic motion embedded in plane Couette turbulence: regeneration cycle and burst. *Journal of Fluid Mechanics*, 449:291–300, December 2001. ISSN 0022-1120,

1469-7645. doi: 10.1017/S0022112001006243. URL https://www.cambridge.org/core/product/identifier/S0022112001006243/type/journal_article.

R.E. Kelly. The Onset and Development of Thermal Convection in Fully Developed Shear Flows. In *Advances in Applied Mechanics*, volume 31, pages 35–112. Elsevier, 1994. ISBN 978-0-12-002031-7. doi: 10.1016/S0065-2156(08)70255-2. URL https://linkinghub.elsevier.com/retrieve/pii/S0065215608702552.

K.J. Kennedy and A. Zebib. Combined free and forced convection between horizontal parallel planes: some case studies. *International Journal of Heat and Mass Transfer*, 26(3):471–474, March 1983. ISSN 00179310. doi: 10.1016/0017-9310(83)90052-2. URL https://linkinghub.elsevier.com/retrieve/pii/0017931083900522.

T. Khapko, T. Kreilos, P. Schlatter, Y. Duguet, B. Eckhardt, and D. S. Henningson. Edge states as mediators of bypass transition in boundary-layer flows. *Journal of Fluid Mechanics*, 801:R2, August 2016. ISSN 0022-1120, 1469-7645. doi: 10.1017/jfm.2016.434. URL https://www.cambridge.org/core/product/identifier/S0022112016004341/type/journal_article.

John Kim, Parviz Moin, and Robert Moser. Turbulence statistics in fully developed channel flow at low Reynolds number. *Journal of Fluid Mechanics*, 177:133–166, April 1987. ISSN 0022-1120, 1469-7645. doi: 10.1017/S0022112087000892. URL https://www.cambridge.org/core/product/identifier/S0022112087000892/type/journal_article.

E.L. Koschmieder and S.G. Pallas. Heat transfer through a shallow, horizontal convecting fluid layer. *International Journal of Heat and Mass Transfer*, 17(9):991–1002, September 1974. ISSN 00179310. doi: 10.1016/0017-9310(74)90181-1. URL https://linkinghub.elsevier.com/retrieve/pii/0017931074901811.

P. D. Lax and A. N. Milgram. IX. Parabolic Equations. In *Contributions to the Theory of Partial Differential Equations. (AM-33)*, pages 167–190. Princeton University Press, December 1955. ISBN 978-1-4008-8218-2. doi: 10.1515/9781400882182-010. URL https://www.degruyter.com/document/doi/10.1515/9781400882182-010/html.

P. Le Gal, A. Pocheau, and V. Croquette. Square versus Roll Pattern at Convective Threshold. *Physical Review Letters*, 54(23):2501–2504, June 1985. ISSN 0031-9007. doi: 10.1103/PhysRevLett.54.2501. URL https://link.aps.org/doi/10.1103/PhysRevLett.54.2501.

Jun Liu and Guenter Ahlers. Spiral-Defect Chaos in Rayleigh-Bénard Convection with Small Prandtl Numbers. *P H Y S I C A L R E V I E W L E T T E R S*, 77(15), 1996.

Mary Lowe and J. P. Gollub. Pattern Selection near the Onset of Convection: The Eckhaus Instability. *Physical Review Letters*, 55(23):2575–2578, December 1985. ISSN 0031-9007. doi: 10.1103/PhysRevLett.55.2575. URL https://link.aps.org/doi/10.1103/PhysRevLett.55.2575.

J-M Luijkx, Jean Karl Platten, and J Cl Legros. On the existence of thermoconvective rolls, transverse to a superimposed mean Poiseuille flow. *International Journal of Heat and Mass Transfer*, 24(7): 1287–1291, 1981. ISSN 0017-9310. Publisher: Elsevier.

Dong-Jun Ma, De-Jun Sun, and Xie-Yuan Yin. Multiplicity of steady states in cylindrical Rayleigh-Bénard convection. *Physical Review E*, 74(3):037302, September 2006. ISSN 1539-3755, 1550-2376. doi: 10.1103/PhysRevE.74.037302. URL https://link.aps.org/doi/10.1103/PhysRevE.74.037302.

Paul Manneville. Rayleigh-Bénard Convection: Thirty Years of Experimental, Theoretical, and Modeling Work. In Gerhard Höhler, Johann H. Kühn, Thomas Müller, Joachim Trümper, Andrei Ruckenstein, Peter Wölfle, Frank Steiner, Innocent Mutabazi, José Eduardo Wesfreid, and Etienne Guyon, editors, *Dynamics of Spatio-Temporal Cellular Structures*, volume 207, pages 41–65. Springer New York, New York, NY, 2006. ISBN 978-0-387-40098-3 978-0-387-25111-0. doi: 10.1007/978-0-387-25111-0_3. URL http://link.springer.com/10.1007/978-0-387-25111-0_3. Series Title: Springer Tracts in Modern Physics.

Á. Meseguer and L.N. Trefethen. Linearized pipe flow to Reynolds number 107. *Journal of Computational Physics*, 186(1):178–197, March 2003. ISSN 00219991. doi: 10.1016/S0021-9991(03)00029-9. URL https://linkinghub.elsevier.com/retrieve/pii/S0021999103000299.

Stephen W. Morris, Eberhard Bodenschatz, David S. Cannell, and Guenter Ahlers. Spiral defect chaos in large aspect ratio Rayleigh-Bénard convection. *Physical Review Letters*, 71(13):2026–2029, September 1993. ISSN 0031-9007. doi: 10.1103/PhysRevLett.71.2026. URL https://link.aps.org/doi/10.1103/PhysRevLett.71.2026.

Stephen W. Morris, Eberhard Bodenschatz, David S. Cannell, and Guenter Ahlers. The spatio-temporal structure of spiral-defect chaos. *Physica D: Nonlinear Phenomena*, 97(1-3):164–179, October 1996. ISSN 01672789. doi: 10.1016/0167-2789(96)00096-6. URL https://linkinghub.elsevier.com/retrieve/pii/0167278996000966.

H. W. Müller, M. Lücke, and M. Kamps. Transversal convection patterns in horizontal shear flow. *Physical Review A*, 45(6):3714–3726, March 1992. ISSN 1050-2947, 1094-1622. doi: 10.1103/PhysRevA.45.3714. URL https://link.aps.org/doi/10.1103/PhysRevA.45.3714.

M. Nagata. Three-dimensional finite-amplitude solutions in plane Couette flow: bifurcation from infinity. *Journal of Fluid Mechanics*, 217:519–527, August 1990. ISSN 0022-1120, 1469-7645. doi: 10.1017/S0022112090000829. URL https://www.cambridge.org/core/product/identifier/S0022112090000829/type/journal_article.

M. Nagata. Three-dimensional traveling-wave solutions in plane Couette flow. *Physical Review E*, 55(2):2023–2025, February 1997. ISSN 1063-651X, 1095-3787. doi: 10.1103/PhysRevE.55.2023. URL https://link.aps.org/doi/10.1103/PhysRevE.55.2023.

X. Nicolas, A. Mojtabi, and J. K. Platten. Two-dimensional numerical analysis of the Poiseuille–Bénard flow in a rectangular channel heated from below. *Physics of Fluids*, 9(2):337–348, February 1997. ISSN 1070-6631, 1089-7666. doi: 10.1063/1.869235. URL https://pubs.aip.org/pof/article/9/2/337/259822/Two-dimensional-numerical-analysis-of-the.

X. Nicolas, J.-M. Luijkx, and J.-K. Platten. Linear stability of mixed convection flows in horizontal rectangular channels of finite transversal extension heated from below. *International Journal of Heat and Mass Transfer*, 43(4):589–610, February 2000. ISSN 00179310. doi: 10.1016/S0017-9310(99)00099-X. URL https://linkinghub.elsevier.com/retrieve/pii/S001793109900099X.

Xavier Nicolas. Revue bibliographique sur les écoulements de Poiseuille–Rayleigh–Bénard : écoulements de convection mixte en conduites rectangulaires horizontales chauffées par le bas. *International Journal of Thermal Sciences*, 41(10):961–1016, October 2002. ISSN 12900729. doi: 10.1016/S1290-0729(02)01374-1. URL https://linkinghub.elsevier.com/retrieve/pii/S1290072902013741.

Xavier Nicolas, Shihe Xin, and Noussaiba Zoueidi. Characterisation of a Wavy Convective Instability in Poiseuille-Rayleigh-Be´nard Flows: Linear Stability Analysis and Non Linear Numerical Simulations Under Random Excitations. In *2010 14th International Heat Transfer Conference, Volume 7*, pages 203–208, Washington, DC, USA, January 2010. ASMEDC. ISBN 978-0-7918-4942-2 978-0-7918-3879-2. doi: 10.1115/IHTC14-22256. URL https://asmedigitalcollection.asme.org/IHTC/proceedings/IHTC14/49422/203/360332.

Xavier Nicolas, Noussaiba Zoueidi, and Shihe Xin. Influence of a white noise at channel inlet on the parallel and wavy convective instabilities of Poiseuille-Rayleigh-Bénard flows. *Physics of Fluids*, 24(8):084101, August 2012. ISSN 1070-6631, 1089-7666. doi: 10.1063/1.4737652. URL https://pubs.aip.org/pof/article/24/8/084101/258132/Influence-of-a-white-noise-at-channel-inlet-on-the.

William M'F. Orr. The Stability or Instability of the Steady Motions of a Perfect Liquid and of a Viscous Liquid. Part II: A Viscous Liquid. *Proceedings of the Royal Irish Academy. Section A: Mathematical and Physical Sciences*, 27:69–138, 1907. ISSN 00358975. URL http://www.jstor.org/stable/20490591. Publisher: Royal Irish Academy.

Steven A. Orszag. Accurate solution of the Orr–Sommerfeld stability equation. *Journal of Fluid Mechanics*, 50(4):689–703, December 1971. ISSN 0022-1120, 1469-7645. doi: 10.1017/S0022112071002842. URL https://www.cambridge.org/core/product/identifier/S0022112071002842/type/journal_article.

Steven A. Orszag, Moshe Israeli, and Michel O. Deville. Boundary conditions for incompressible flows. *Journal of Scientific Computing*, 1(1):75–111, 1986. ISSN 0885-7474, 1573-7691. doi: 10.1007/BF01061454. URL http://link.springer.com/10.1007/BF01061454.

S. Ostrach and Y. Kamotani. Heat Transfer Augmentation in Laminar Fully Developed Channel Flow by Means of Heating From Below. *Journal of Heat Transfer*, 97(2):220–225, May 1975. ISSN 0022-1481, 1528-8943. doi: 10.1115/1.3450344. URL https://asmedigitalcollection.asme.org/heattransfer/article/97/2/220/416581/Heat-Transfer-Augmentation-in-Laminar-Fully.

MT Ouazzani, Jean-Paul Caltagirone, Gilles Meyer, and Abdelkader Mojtabi. Etude numerique et expérimentale de la convection mixte entre deux plans horizontaux à températures différentes. *International journal of heat and mass transfer*, 32(2):261–269, 1989. ISSN 0017-9310. Publisher: Elsevier.

MT Ouazzani, Jean Karl Platten, and Abdelkader Mojtabi. Etude expérimentale de la convection mixte entre deux plans horizontaux à températures différentes—II. *International journal of heat and mass transfer*, 33(7):1417–1427, 1990. ISSN 0017-9310. Publisher: Elsevier.

Hervé Pabiou, Xavier Nicolas, Shihe Xin, and Sophie Mergui. Observations d'une instabilité convective apparaissant sous la forme de rouleaux sinueux dans un écoulement de Poiseuille–Rayleigh–Bénard. *Mécanique & industries*, 4(5):537–543, 2003. ISSN 1296-2139. Publisher: Elsevier.

Hervé Pabiou, Sophie Mergui, and Christine Bénard. Wavy secondary instability of longitudinal rolls in RayleighPoiseuille flows. *Journal of Fluid Mechanics*, 542(-1):175, October 2005. ISSN 0022-1120, 1469-7645. doi: 10.1017/S0022112005006154. URL http://www.journals.cambridge.org/abstract_S0022112005006154.

Chaitanya S Paranjape. Onset of turbulence in plane Poiseuille flow. 2019. Publisher: IST Austria Klosterneuburg, Austria.

Chaitanya S. Paranjape, Yohann Duguet, and Björn Hof. Oblique stripe solutions of channel flow. *Journal of Fluid Mechanics*, 897:A7, August 2020. ISSN 0022-1120, 1469-7645. doi: 10.1017/jfm.2020.322. URL https://www.cambridge.org/core/product/identifier/S0022112020003225/type/journal_article.

Chaitanya S. Paranjape, Gökhan Yalnız, Yohann Duguet, Nazmi Burak Budanur, and Björn Hof. Direct Path from Turbulence to Time-Periodic Solutions. *Physical Review Letters*, 131(3):034002, July 2023. ISSN 0031-9007, 1079-7114. doi: 10.1103/PhysRevLett.131.034002. URL https://link.aps.org/doi/10.1103/PhysRevLett.131.034002.

Anthony T Patera. A spectral element method for fluid dynamics: Laminar flow in a channel expansion. *Journal of Computational Physics*, 54(3):468–488, June 1984. ISSN 00219991. doi: 10.1016/0021-9991(84)90128-1. URL https://linkinghub.elsevier.com/retrieve/pii/0021999184901281.

M. R. Paul, M. I. Einarsson, P. F. Fischer, and M. C. Cross. Extensive chaos in Rayleigh-Bénard convection. *Physical Review E*, 75(4):045203, April 2007. ISSN 1539-3755, 1550-2376. doi: 10.1103/PhysRevE.75.045203. URL https://link.aps.org/doi/10.1103/PhysRevE.75.045203.

M.R. Paul, K.-H. Chiam, M.C. Cross, P.F. Fischer, and H.S. Greenside. Pattern formation and dynamics in Rayleigh–Bénard convection: numerical simulations of experimentally realistic geometries. *Physica D: Nonlinear Phenomena*, 184(1-4):114–126, October 2003. ISSN 01672789. doi: 10.1016/S0167-2789(03)00216-1. URL https://linkinghub.elsevier.com/retrieve/pii/S0167278903002161.

Anne Pellew and Richard Vynne Southwell. On maintained convective motion in a fluid heated from below. *Proceedings of the Royal Society of London. Series A. Mathematical and Physical Sciences*, 176(966):312–343, November 1940. ISSN 0080-4630, 2053-9169. doi: 10.1098/rspa.1940.0092. URL https://royalsocietypublishing.org/doi/10.1098/rspa.1940.0092.

Sergio Pirozzoli, Matteo Bernardini, Roberto Verzicco, and Paolo Orlandi. Mixed convection in turbulent channels with unstable stratification. *Journal of Fluid Mechanics*, 821:482–516, June 2017. ISSN 0022-1120, 1469-7645. doi: 10.1017/jfm.2017.216. URL https://www.cambridge.org/core/product/identifier/S0022112017002166/type/journal_article.

Brendan B Plapp and Eberhard Bodenschatz. Core dynamics of multi-armed spirals in Rayleigh-Bénard convection. *Physica Scripta*, T67:111–116, January 1996. ISSN 0031-8949, 1402-4896. doi: 10.1088/0031-8949/1996/T67/022. URL https://iopscience.iop.org/article/10.1088/0031-8949/1996/T67/022.

Brendan B. Plapp, David A. Egolf, Eberhard Bodenschatz, and Werner Pesch. Dynamics and Selection of Giant Spirals in Rayleigh-Bénard Convection. *Physical Review Letters*, 81(24):5334–5337, December 1998. ISSN 0031-9007, 1079-7114. doi: 10.1103/PhysRevLett.81.5334. URL https://link.aps.org/doi/10.1103/PhysRevLett.81.5334.

Brendan Bryce Plapp. Spiral pattern formation in Rayleigh-Benard convection. *Ph.D. Thesis*, page 3118, December 1997. URL https://ui.adsabs.harvard.edu/abs/1997PhDT.....105P.

A. Prigent and O. Dauchot. "Barber pole turbulence" in large aspect ratio Taylor-Couette flow. *Physical Review Letters*, 89(1):014501, June 2002. ISSN 0031-9007, 1079-7114. doi: 10.1103/PhysRevLett.89.014501. URL http://arxiv.org/abs/cond-mat/0009241. arXiv:cond-mat/0009241.

Arnaud Prigent, Guillaume Grégoire, Hugues Chaté, and Olivier Dauchot. Long-wavelength modulation of turbulent shear flows. *Physica D: Nonlinear Phenomena*, 174(1-4):100–113, January 2003. ISSN 01672789. doi: 10.1016/S0167-2789(02)00685-1. URL https://linkinghub.elsevier.com/retrieve/pii/S0167278902006851.

Subhashis Ray and J. Srinivasan. Analysis of conjugate laminar mixed convection cooling in a shrouded array of electronic components. *International Journal of Heat and Mass Transfer*, 35

(4):815–822, April 1992. ISSN 00179310. doi: 10.1016/0017-9310(92)90249-R. URL https://linkinghub.elsevier.com/retrieve/pii/001793109290249R.

Lord Rayleigh. LIX. *On convection currents in a horizontal layer of fluid, when the higher temperature is on the under side*. *The London, Edinburgh, and Dublin Philosophical Magazine and Journal of Science*, 32(192):529–546, December 1916. ISSN 1941-5982, 1941-5990. doi: 10.1080/14786441608635602. URL https://www.tandfonline.com/doi/full/10.1080/14786441608635602.

Satish C. Reddy and Dan S. Henningson. Energy growth in viscous channel flows. *Journal of Fluid Mechanics*, 252:209–238, July 1993. ISSN 0022-1120, 1469-7645. doi: 10.1017/S0022112093003738. URL https://www.cambridge.org/core/product/identifier/S0022112093003738/type/journal_article.

Satish C. Reddy, Peter J. Schmid, and Dan S. Henningson. Pseudospectra of the Orr–Sommerfeld Operator. *SIAM Journal on Applied Mathematics*, 53(1):15–47, February 1993. ISSN 0036-1399, 1095-712X. doi: 10.1137/0153002. URL http://epubs.siam.org/doi/10.1137/0153002.

Florian Reetz and Tobias M. Schneider. Invariant states in inclined layer convection. Part 1. Temporal transitions along dynamical connections between invariant states. *Journal of Fluid Mechanics*, 898:A22, September 2020. ISSN 0022-1120, 1469-7645. doi: 10.1017/jfm.2020.317. URL https://www.cambridge.org/core/product/identifier/S0022112020003171/type/journal_article.

Florian Reetz, Tobias Kreilos, and Tobias M. Schneider. Exact invariant solution reveals the origin of self-organized oblique turbulent-laminar stripes. *Nature Communications*, 10(1):2277, May 2019. ISSN 2041-1723. doi: 10.1038/s41467-019-10208-x. URL https://doi.org/10.1038/s41467-019-10208-x.

Florian Reetz, Priya Subramanian, and Tobias M. Schneider. Invariant states in inclined layer convection. Part 2. Bifurcations and connections between branches of invariant states. *Journal of Fluid Mechanics*, 898:A23, September 2020. ISSN 0022-1120, 1469-7645. doi: 10.1017/jfm.2020.318. URL https://www.cambridge.org/core/product/identifier/S0022112020003183/type/journal_article.

Osborne Reynolds. XXIX. An experimental investigation of the circumstances which determine whether the motion of water shall be direct or sinuous, and of the law of resistance in parallel channels. *Philosophical Transactions of the Royal Society of London*, 174:935–982, December 1883. ISSN 0261-0523, 2053-9223. doi: 10.1098/rstl.1883.0029. URL https://royalsocietypublishing.org/doi/10.1098/rstl.1883.0029.

Osborne Reynolds. IV. On the dynamical theory of incompressible viscous fluids and the determination of the criterion. *Philosophical Transactions of the Royal Society of London. (A.)*, 186:123–164, December 1895. ISSN 0264-3820, 2053-9231. doi: 10.1098/rsta.1895.0004. URL https://royalsocietypublishing.org/doi/10.1098/rsta.1895.0004.

H. T. Rossby. A study of Bénard convection with and without rotation. *Journal of Fluid Mechanics*, 36(2):309–335, April 1969. ISSN 0022-1120, 1469-7645. doi: 10.1017/S0022112069001674. URL https://www.cambridge.org/core/product/identifier/S0022112069001674/type/journal_article.

Sten Rüdiger and Fred Feudel. Pattern formation in Rayleigh-Bénard convection in a cylindrical container. *Physical Review E*, 62(4):4927–4931, October 2000. ISSN 1063-651X, 1095-3787. doi: 10.1103/PhysRevE.62.4927. URL https://link.aps.org/doi/10.1103/PhysRevE.62.4927.

A. Scagliarini, H. Einarsson, Á. Gylfason, and F. Toschi. Law of the wall in an unstably stratified turbulent channel flow. *Journal of Fluid Mechanics*, 781:R5, October 2015. ISSN 0022-1120, 1469-7645. doi: 10.1017/jfm.2015.498. URL https://www.cambridge.org/core/product/identifier/S002211201500498X/type/journal_article.

Andrea Scagliarini, Armann Gylfason, and Federico Toschi. Heat flux scaling in turbulent Rayleigh-Bénard convection with an imposed longitudinal wind. *Physical Review E*, 89(4):043012, April 2014. ISSN 1539-3755, 1550-2376. doi: 10.1103/PhysRevE.89.043012. URL http://arxiv.org/abs/1311.4598. arXiv:1311.4598 [physics].

H. Schlichting. Zur Enstehung der Turbulenz bei der Plattenströmung. *Nachrichten von der Gesellschaft der Wissenschaften zu Göttingen, Mathematisch-Physikalische Klasse*, 1933:181–208, 1933. URL http://eudml.org/doc/59420.

Hermann Schlichting and Klaus Gersten. Onset of Turbulence (Stability Theory). In *Boundary-Layer Theory*, pages 415–496. Springer Berlin Heidelberg, Berlin, Heidelberg, 2017. ISBN 978-3-662-52917-1 978-3-662-52919-5. doi: 10.1007/978-3-662-52919-5_15. URL http://link.springer.com/10.1007/978-3-662-52919-5_15.

A. Schlüter, D. Lortz, and F. Busse. On the stability of steady finite amplitude convection. *Journal of Fluid Mechanics*, 23(01):129, September 1965. ISSN 0022-1120, 1469-7645. doi: 10.1017/S0022112065001271. URL http://www.journals.cambridge.org/abstract_S0022112065001271.

Peter J. Schmid. Nonmodal Stability Theory. *Annual Review of Fluid Mechanics*, 39(1):129–162, January 2007. ISSN 0066-4189, 1545-4479. doi: 10.1146/annurev.fluid.38.050304.092139. URL https://www.annualreviews.org/doi/10.1146/annurev.fluid.38.050304.092139.

Peter J. Schmid and Dan S. Henningson. *Stability and Transition in Shear Flows*, volume 142 of *Applied Mathematical Sciences*. Springer New York, New York, NY, 2001. ISBN 978-1-4612-6564-1 978-1-4613-0185-1. doi: 10.1007/978-1-4613-0185-1. URL http://link.springer.com/10.1007/978-1-4613-0185-1.

Rainer Schmitz, Werner Pesch, and Walter Zimmermann. Spiral-defect chaos: Swift-Hohenberg model versus Boussinesq equations. *Physical Review E*, 65(3):037302, March 2002. ISSN 1063-651X, 1095-3787. doi: 10.1103/PhysRevE.65.037302. URL https://link.aps.org/doi/10.1103/PhysRevE.65.037302.

Tobias M. Schneider, Bruno Eckhardt, and James A. Yorke. Turbulence transition and the edge of chaos in pipe flow. *Physical Review Letters*, 99(3):034502, July 2007. ISSN 0031-9007, 1079-7114. doi: 10.1103/PhysRevLett.99.034502. URL http://arxiv.org/abs/nlin/0703067. arXiv:nlin/0703067.

Masaki Shimizu and Paul Manneville. Bifurcations to turbulence in transitional channel flow. *Physical Review Fluids*, 4(11):113903, November 2019. doi: 10.1103/PhysRevFluids.4.113903. URL https://link.aps.org/doi/10.1103/PhysRevFluids.4.113903. Publisher: American Physical Society.

Jennifer H. Siggers. Dynamics of target patterns in low-Prandtl-number convection. *Journal of Fluid Mechanics*, 475:357–375, January 2003. ISSN 0022-1120, 1469-7645. doi: 10.1017/S0022112002002896. URL https://www.cambridge.org/core/product/identifier/S0022112002002896/type/journal_article.

Joseph D. Skufca, James A. Yorke, and Bruno Eckhardt. Edge of Chaos in a Parallel Shear Flow. *Physical Review Letters*, 96(17):174101, May 2006. ISSN 0031-9007, 1079-7114. doi: 10.1103/PhysRevLett.96.174101. URL https://link.aps.org/doi/10.1103/PhysRevLett.96.174101.

Arnold Sommerfeld. *Ein beitrag zur hydrodynamischen erklaerung der turbulenten fluessigkeitsbewegungen*. 1909.

Baofang Song, Dwight Barkley, Björn Hof, and Marc Avila. Speed and structure of turbulent fronts in pipe flow. *Journal of Fluid Mechanics*, 813:1045–1059, February 2017. ISSN 0022-1120, 1469-7645. doi: 10.1017/jfm.2017.14. URL https://www.cambridge.org/core/product/identifier/S0022112017000143/type/journal_article.

Herbert Brian Squire. On the stability for three-dimensional disturbances of viscous fluid flow between parallel walls. *Proceedings of the Royal Society of London. Series A, Containing Papers of a Mathematical and Physical Character*, 142(847):621–628, November 1933. ISSN 0950-1207, 2053-9150. doi: 10.1098/rspa.1933.0193. URL https://royalsocietypublishing.org/doi/10.1098/rspa.1933.0193.

J. Swift and P. C. Hohenberg. Hydrodynamic fluctuations at the convective instability. *Physical Review A*, 15(1):319–328, January 1977. ISSN 0556-2791. doi: 10.1103/PhysRevA.15.319. URL https://link.aps.org/doi/10.1103/PhysRevA.15.319.

J. J. Tao, Bruno Eckhardt, and X. M. Xiong. Extended localized structures and the onset of turbulence in channel flow. *Physical Review Fluids*, 3(1):011902, January 2018. doi: 10.1103/PhysRevFluids.3.

011902. URL https://link.aps.org/doi/10.1103/PhysRevFluids.3.011902. Publisher: American Physical Society.

W. Tollmien. Über die Entstehung der Turbulenz. 1. Mitteilung. *Nachrichten von der Gesellschaft der Wissenschaften zu Göttingen, Mathematisch-Physikalische Klasse*, 1929:21–44, 1928. URL http://eudml.org/doc/59276.

Lloyd N. Trefethen. Pseudospectra of Linear Operators. *SIAM Review*, 39(3):383–406, January 1997. ISSN 0036-1445, 1095-7200. doi: 10.1137/S0036144595295284. URL http://epubs.siam.org/doi/10.1137/S0036144595295284.

Takahiro Tsukahara, Kaoru Iwamoto, Hiroshi Kawamura, and Tetsuaki Takeda. DNS of heat transfer in a transitional channel flow accompanied by a turbulent puff-like structure, September 2014a. URL http://arxiv.org/abs/1406.0586. arXiv:1406.0586 [physics].

Takahiro Tsukahara, Yasuo Kawaguchi, and Hiroshi Kawamura. An experimental study on turbulent-stripe structure in transitional channel flow, 2014b. URL https://arxiv.org/abs/1406.1378. Version Number: 2.

Takahiro Tsukahara, Yohji Seki, Hiroshi Kawamura, and Daisuke Tochio. DNS of turbulent channel flow at very low Reynolds numbers, September 2014c. URL http://arxiv.org/abs/1406.0248. arXiv:1406.0248 [physics].

Laurette S. Tuckerman and Dwight Barkley. Global Bifurcation to Traveling Waves in Axisymmetric Convection. *Physical Review Letters*, 61(4):408–411, July 1988. ISSN 0031-9007. doi: 10.1103/PhysRevLett.61.408. URL https://link.aps.org/doi/10.1103/PhysRevLett.61.408.

Laurette S. Tuckerman and Dwight Barkley. Bifurcation Analysis for Timesteppers. In *Numerical Methods for Bifurcation Problems and Large-Scale Dynamical Systems*, volume 119, pages 453–466. Springer New York, New York, NY, 2000. ISBN 978-1-4612-7044-7 978-1-4612-1208-9. doi: 10.1007/978-1-4612-1208-9_20. URL http://link.springer.com/10.1007/978-1-4612-1208-9_20. Series Title: The IMA Volumes in Mathematics and its Applications.

Laurette S Tuckerman and Dwight Barkley. Patterns and dynamics in transitional plane Couette flow. *Physics of Fluids*, 23(4), 2011. ISSN 1070-6631. Publisher: AIP Publishing.

Laurette S. Tuckerman, Tobias Kreilos, Hecke Schrobsdorff, Tobias M. Schneider, and John F. Gibson. Turbulent-laminar patterns in plane Poiseuille flow. *Physics of Fluids*, 26(11):114103, November 2014. ISSN 1070-6631, 1089-7666. doi: 10.1063/1.4900874. URL https://pubs.aip.org/pof/article/26/11/114103/315350/Turbulent-laminar-patterns-in-plane-Poiseuille.

Geoffrey K. Vallis, Douglas J. Parker, and Steven M. Tobias. A simple system for moist convection: the Rainy–Bénard model. *Journal of Fluid Mechanics*, 862:162–199, March 2019. ISSN 0022-1120, 1469-7645. doi: 10.1017/jfm.2018.954. URL https://www.cambridge.org/core/product/identifier/S0022112018009540/type/journal_article.

Milton Van Dyke and Milton Van Dyke. *An album of fluid motion*, volume 176. Parabolic Press Stanford, 1982.

D. Viswanath. Recurrent motions within plane Couette turbulence. *Journal of Fluid Mechanics*, 580:339–358, June 2007. ISSN 0022-1120, 1469-7645. doi: 10.1017/S0022112007005459. URL https://www.cambridge.org/core/product/identifier/S0022112007005459/type/journal_article.

Eduardo Vitral, Saikat Mukherjee, Perry H. Leo, Jorge Viñals, Mark R. Paul, and Zhi-Feng Huang. Spiral defect chaos in Rayleigh-Bénard convection: Asymptotic and numerical studies of azimuthal flows induced by rotating spirals. *Physical Review Fluids*, 5(9):093501, September 2020. ISSN 2469-990X. doi: 10.1103/PhysRevFluids.5.093501. URL https://link.aps.org/doi/10.1103/PhysRevFluids.5.093501.

Fabian Waleffe. Exact coherent structures in channel flow. *Journal of Fluid Mechanics*, 435:93–102, May 2001. ISSN 0022-1120, 1469-7645. doi: 10.1017/S0022112001004189. URL https://www.cambridge.org/core/product/identifier/S0022112001004189/type/journal_article.

Fabian Waleffe. Homotopy of exact coherent structures in plane shear flows. *Physics of Fluids*, 15(6):1517–1534, June 2003. ISSN 1070-6631, 1089-7666. doi: 10.1063/1.1566753. URL https://pubs.aip.org/pof/article/15/6/1517/448391/Homotopy-of-exact-coherent-structures-in-plane.

José Eduardo Wesfreid. Henri Bénard: Thermal convection and vortex shedding. *Comptes Rendus. Mécanique*, 345(7):446–466, June 2017. ISSN 1873-7234. doi: 10.1016/j.crme.2017.06.006. URL https://comptes-rendus.academie-sciences.fr/mecanique/articles/10.1016/j.crme.2017.06.006/.

G. E. Willis and J. W. Deardorff. The oscillatory motions of Rayleigh convection. *Journal of Fluid Mechanics*, 44(04):661, December 1970. ISSN 0022-1120, 1469-7645. doi: 10.1017/S0022112070002070. URL http://www.journals.cambridge.org/abstract_S0022112070002070.

Hao-wen Xi, J. D. Gunton, and Jorge Viñals. Spiral defect chaos in a model of Rayleigh-Bénard convection. *Physical Review Letters*, 71(13):2030–2033, September 1993. ISSN 0031-9007. doi: 10.1103/PhysRevLett.71.2030. URL https://link.aps.org/doi/10.1103/PhysRevLett.71.2030.

Haowen Xi and J. D. Gunton. Spatiotemporal chaos in a model of Rayleigh-Bénard convection. *Physical Review E*, 52(5):4963–4975, November 1995. ISSN 1063-651X, 1095-3787. doi: 10.1103/PhysRevE.52.4963. URL https://link.aps.org/doi/10.1103/PhysRevE.52.4963.

Xiangkai Xiao and Baofang Song. The growth mechanism of turbulent bands in channel flow at low Reynolds numbers. *Journal of Fluid Mechanics*, 883:R1, January 2020. ISSN 0022-1120,

1469-7645. doi: 10.1017/jfm.2019.899. URL https://www.cambridge.org/core/product/identifier/S0022112019008991/type/journal_article.

Shihe Xin, Xavier Nicolas, and Patrick Le Quéré. Stability analyses of Longitudinal Rolls of Poiseuille-Rayleigh-Bénard Flows in Air-Filled Channels of Finite Transversal Extension. *Numerical Heat Transfer, Part A: Applications*, 50(5):467–490, July 2006. ISSN 1040-7782, 1521-0634. doi: 10.1080/10407780600620079. URL http://www.tandfonline.com/doi/abs/10.1080/10407780600620079.

Xiangming Xiong, Jianjun Tao, Shiyi Chen, and Luca Brandt. Turbulent bands in plane-Poiseuille flow at moderate Reynolds numbers. *Physics of Fluids*, 27(4):041702, April 2015. ISSN 1070-6631, 1089-7666. doi: 10.1063/1.4917173. URL https://pubs.aip.org/pof/article/27/4/041702/1019208/Turbulent-bands-in-plane-Poiseuille-flow-at.